# Reducing the emission of climate-altering substances in cementitious materials: A comparison between alkali-activated materials and Portland cement-based composites incorporating recycled tire rubber

Marco Valente[1,2*], Matteo Sambucci[1,2], Mehdi Chougan[3], Seyed Hamidreza Ghaffar[3]

[1] *Department of Chemical Engineering, Materials, Environment, Sapienza University of Rome, 00184 Rome*

[2] *INSTM Reference Laboratory for Engineering of Surface Treatments, Department of Chemical Engineering, Materials, Environment, Sapienza University of Rome, 00184 Rome, Italy*

[3] *Department of Civil and Environmental Engineering, Brunel University, London, Uxbridge, Middlesex, UB 8 3PH, United Kingdom*

[*]Corresponding author: **marco.valente@uniroma1.it**

## Keywords

Eco-sustainable construction materials; Ground tire rubber; Geopolymer; OPC; Rubberized mortars; Microstructural analysis; Mechanical tests; Porosity; Water absorption.

## Abstract

Low carbon or near-zero carbon concrete technology is in line with the pillars of sustainable development, where industrial waste or low-carbon binders can reduce or eliminate consumption of Portland cement and natural resources, leading to less environmental pollution. This work presents an experimental study on the comparison between alkali-activated materials (also recognized ad geopolymers) and a traditional cementitious matrix (Portland cement) incorporated with rubber particles, deriving from end-of-life tires, as replacement of raw mineral aggregates. To explore the potential of rubber-geopolymer compounds, an experimental comparative analysis with rubber-Portland mortars was performed. Initial investigations (microstructural/compositional analysis, porosity and water absorption measurements, and mechanical tests) were conducted on rubberized samples obtained by varying the binder, the sand-rubber replacement ratio (0 vol.%, 50 vol.%, and 100 vol.%) and the rubber particle size (0-1 mm rubber fine aggregate and 1-3 mm rubber granules). The results revealed a greater compatibility of the alkali-activated matrix with tire rubber aggregates, resulting in better performance in terms of interfacial adhesion, reduced porosity rate, flexural strength, and toughness. However, compressive strength results showed a weaker mechanical performance of rubber-geopolymer mixes compared to Portland counterparts. As also verified by Si/Al elemental analysis, the structural quality and mechanical development of the geopolymer matrix was strongly influenced by the removal of sand as a Si-source. The potential embodied carbon emission performance and cost analysis were also estimated to evaluate the economic and environmental impact related to the use of recycled rubber as complete aggregate in Portland and geopolymer mixes. Sustainability analysis revealed the greater environmental friendliness of geopolymer formulations compared to those in ordinary cement, but higher production costs. The total addition of rubber aggregates induced an increase in emissions and costs (variable according to the type of matrix) which, however, does not directly correlate with the processing/price of the polymer fraction. Deepening the research on cleaner matrices and promoting the use of recycled materials in concrete applications could lead to a gap levelling between Portland and geopolymer rubber-based composites. Building on these findings, future study will focus on the optimization of the mix design as a function of rubber aggregates.

# 1. Introduction

The decrease of greenhouse gases is currently one of civilization's most pressing challenges. To address this issue, all industrial sectors, which account for 25% of global carbon footprint, must be included. This is especially true for the cement industry, which accounts for around 7% of all Carbon dioxide ($CO_2$) emissions in the environment (Damineli et al., 2010; Ali et al., 2011). Accordingly, improving the sustainability in cement and concrete industries is a crucial challenge for environmental well-being and human development. The production of ordinary Portland cement (OPC), the main constituent of concrete, leads to the $CO_2$ release and other greenhouse gases, including Nitrogen oxides ($NO_x$), Sulphur dioxide ($SO_2$), and particulate matter (Naik, 2005). About 8-10 % of global anthropogenic emissions are related to OPC manufacturing. It is estimated that one ton of cement releases almost 0.816 ton of $CO_2$ (Sheheryar et al., 2021). Due to the growing industrialization, urbanization, and infrastructure development, OPC demand is on the rise: cement production is expected to be around 5 Gt by 2050 (Sheheryar et al., 2021). In a long-term forecast, however, it must be considered that during the entire lifecycle of concrete, the carbonation, a physicochemical process in which the cement hydration products gradually reabsorb atmospheric $CO_2$, significantly affects the overall carbon footprint. As verified by Xi et al. (2016), a cumulative amount of 4.5 Gt of $CO_2$ has been sequestered in carbonating cement materials from 1930 to 2013, offsetting 43% of the carbon emissions from production of cement over the same period. However, the environmental impact not only involves the polluting emission and ozone-depleting effects, but also includes additional factors such as energy consumption and natural resources exploitation. Thermal and electrical energy are both needed during the OPC production process (extraction of raw materials from quarries, grinding process, kiln operation, fuel consumption), resulting in thermal energy consumption and total electricity requirement of about 4-6 GJ and 130-150 kWh per ton of cement, respectively (Golewsky, 2020). Finally, the depletion of natural aggregates (sand, gravel, gypsum) and water is also a current environmental problem in the cement-based materials context. Extensive mining activities have direct consequences on the ecosystems, causing soil and riverbed erosion, changing in river courses, and decreasing the underground aquifers. In addition, the reduced availability of freshwater (only 2.5 % of the global rate), commonly employed for concrete manufacturing, is a fundamental aspect to consider in terms of resources safeguard and eco-friendly development (Dhondy et al., 2019). Recently, the European Environmental Agency (EEA 2020) defined some key actions to mitigate the adverse environmental impact of the construction sector, aiming to cut the greenhouse emission up to 60% by 2050 and preserve the natural resources. Investing in “greener” cementitious binders and promoting the use of recycled materials and industrial by-products as secondary raw materials represent the principal topics of the EEA proposal.

In the 1970s, the term "geopolymer" was introduced to describe the type of solid materials developed by reacting an aluminosilicate powder with an alkaline solution, which is generally a mixture of Sodium or Potassium hydroxide (NaOH, KOH) and Sodium or Potassium silicate ($Na_2SiO_3$, $K_2O_3Si$) (Davidovits, 1982). The Silicon (Si) and Aluminum (Al)-rich source materials used in geopolymer production can be of geological origin (pumice, zeolites, volcanic ash) or by-products of industrial activities, such as fly ash (FA), metakaolin (MK), or ground granulated blast furnace slag (GGBS) (Sambucci et al., 2021). Due to the increasingly intensive experimentation on geopolymeric materials, some of these secondary resources (FA and slag) have now become traditional precursors and are available on the market. Since different raw materials provide different chemical composition, binary or ternary blends of aluminosilicate precursors are usually used in the production of AAMs, also allowing to tailor the final material, in terms of performance and costs, for a given application (Duxson et al., 2007). As reported by Provis and Van Deventer (2009), the synthesis process generates a geopolymeric gel binder phase, which is a disordered alkali aluminosilicate gel phase. Unreacted solid binder particles are embedded inside this phase, and the porous network of the gel accommodates the water required to mix the binders provided by the alkaline solution. Aluminate and silicate tetrahedra form a three-dimensional network structure in the gel phase. Due to $Al^{3+}$ in four-fold coordination positioned on one

or more of the bridging oxygens in each aluminate tetrahedron, this network possesses a negative charge that is balanced by alkali metal cations supplied by the activator solution.

The principles of geopolymer technology are based on the pioneering research conducted in the 1950s by Victor Glukhovsky on the synthesis of alkali-activated materials (AAM) obtained by mixing natural raw materials (rocks and volcanic ash) with alkaline activating solution (Marvila et al., 2021). Because of this chemistry similarity, "geopolymers" and "AAMs" nomenclatures are equally accepted by the research community. In the mid 1990's, the study conducted by Wastiels et al. (1994) highlighted the potential of these materials as feedstock in the construction industry, leading, in the past few decades, many researchers to recognize geopolymer concrete (GPC), obtained by mixing fine and/or coarse mineral aggregates with AAM-based cement, as a valuable and sustainable alternative to OPC. Firstly, the benefits associated with GPC-based materials include the decrease in $CO_2$ footprint, the low depletion of natural resources by the supply of industrial wastes as raw materials, and the reduced levels of energy requirements both for precursors manufacturing and heat for material curing (up to 40% reduction in overall energy consumption) (Zhang et al., 2020; Amran et al., 2021). Some life cycle assessment (LCA) studies demonstrated the great potential for geopolymer materials to mitigate the climate change impacts of cement production. According to McLellan et al. (2011), based on typical Australian feedstocks, an estimated 44–64% improvement in greenhouse gas emissions over OPC can be achieved. Such results are realisable by an appropriate selection of raw material sources and optimizing the cost of transportation. The broad range of potential feedstock sources leads to a very wide range of potential impacts: compared with emissions from OPC materials, emissions from geopolymer concrete can be 97% lower up to 14% higher. Ouellet-Plamondon and Habert (2015) demonstrated a promising environmental performance for ''one-part'' geopolymer cement, which showed carbon footprint levels much lower than Portland cement-based mixtures (about 93% reduction in global warming potential). Recently, Meshram and Kumar (2021) evaluated the eco-impact of geopolymer cement production in comparison to Portland cement manufacturing, by considering the Indian scenario which is recognized as the second-leading cement producer in the world. In agreement with the LCA results, the geopolymer cement reduces the global warming potential by 70%, abiotic depletion potential fossil by 49%, abiotic depletion potential element by 34%, and terrestrial ecotoxicity potential by 77% when compared with OPC of the construction industry. In terms of engineering properties, GPC provides highly functional and competitive performance compared to OPC-based materials. Faster setting time, higher early strength, greater durability to acid attack, and higher fire resistance are some of the potential peculiarities of geopolymeric mixes with respect to Portland ones. As an advantage, geopolymers exhibit superior mechanical and physical properties. Moreover, these materials are known as low-carbon alternatives to Portland cement, consuming vast quantities of industrial waste and by-products while diminishing greenhouse gas emissions. Due to their advantages, this category of cementitious materials could be employed in fire-resistant fibre composites, concrete infrastructures, sealants, and ceramics (Sambucci et al., 2021a; Nath and Kumar, 2020; Nuruddin et al., 2016).

Although attractive discoveries have been detected over the years, geopolymer technology faces numerous challenges for full integration into the global concrete materials industry. One of the main limitations is the absence of technical standards which should be created by a global committee. Proper standard codes that consider the performance as a base for concrete evaluation may be the most suitable solution for the adaptation of such new materials. Added to this is the question of the long-term behaviour (mechanical and durability performances) of these materials. Generally, civil and building engineering request at least 30 years of real-world verification before such concrete materials are adapted for the construction industries. Lack of data makes them unsuitable where the safety of the user is a critical concern (Part et al., 2015). Another potential challenge in commercializing geopolymers technology is the inconsistency in properties and characteristics shown by various geopolymer source materials. The performance of geopolymers is governed by the properties of the source material itself (chemical composition and physical properties). Popular source

materials originated from industry wastes (such as FA, GGBS, rice husk ash) have their own unique physico-chemical properties thus require distinctly different alkaline activator dosage and processing methods to reach similar performance. As mentioned above, the features of the same source materials, but from different locations possessed different characteristics in terms of chemical composition and physical properties. The aforementioned variations will pose problems in terms of reproducibility and when transferring geopolymer knowledge to the industrial practitioners, making it more difficult for consumers to accept new concrete technologies and manufacturing methods (Wang et al., 2019). Based on the close interdependence between the nature and characteristics of aluminosilicate source materials, the synthesis parameters, and the properties of the final product, some studies revealed potential issues that need to be addressed in the production of these materials. As researched by Wang et al. (2019), the incomplete consumption of alkaline and/or soluble silicates, due to the existence of dissolution equilibrium of raw aluminosilicate in the activating solution, results in efflorescence phenomena and consequent porous and permeable microstructure in the hardened material. A well-designed mix proportions or an adequate thermal activation can eliminate/mitigate the efflorescence in GPC. Van Deventer et al. (2012) highlighted the pivotal role of Calcium (Ca) availability in aluminosilicate precursors and its ease of dissolution under alkaline activation on the engineering and durability properties of the geopolymer materials. As demonstrated by Fernandez-Jimenez and Palomo (2012), Ca content, deriving from the precursors or aggregates, also has a significant contribution to the structural expansion of AAMs. Ca-poor geopolymeric phases reduce or may even prevent the alkali-silica reaction process and consequent damage due to expansion. Pacheco-Torgal et al. (2017) reviewed that geopolymer mixtures are more prone to alkali leaching than OPC mixes, which could lead to a rapid and disastrous reduction in the pH, causing steel reinforcements corrosion. However, Ca-rich mixtures have much lower diffusion coefficients and a more tortuous pore system that hinders the movements of ions through the paste, extending the long-term durability. In this regard, a complete elucidation of geopolymerization reaction kinetics and chemistry based on different source materials could be useful as a general guideline for the geopolymers researchers in identifying the crucial parameters and factors to be considered during the design and fabrication stage. Recent progress in this research field led to the development of analytical investigations based on thermodynamic simulations aiming at studying the phase assemblages of reaction products of AAMs, which are highly influenced by the chemistry of precursor and activator, and gaining insight into selection of raw materials (Xiao et al., 2020a). For instance, thermodynamic modelling was successfully implemented by Xiao et al. (2021) to analyze the influence of waste glass as a novel precursor material for AAMs and, predicting a relationship between phase assemblages and mechanical strength properties in the synthesized binders.

To further enhance the eco-sustainability and engineering functionality of geopolymer technology, recent research is focusing on the optimization of geopolymeric mix designs, by replacing common natural reinforcing aggregates (sand, gravel, stone) with recycled waste materials (Mohajerani et al., 2019). Lim et al. (2021) synthesized FA-based GPC using grounded waste marble (GWM) as a substitute to natural aggregates to reduce the adverse environmental impact caused by marble industry activities (mining and processing). The authors demonstrated the possibility of replacing up to 50 wt% of the natural fraction obtaining higher mechanical and permeability resistance than the control (0 wt% GWM) mix. Dave et al. (2017) observed excellent impact resistance and energy absorption in FA-based GPC containing waste plastic granules (WPGs) to replace 10 wt% of sand (up to 10% improvement in drop impact strength). De Rossi et al. (2019) employed construction and demolition waste (CDW) as fine aggregates in FA-MK geopolymer mortars, leading to an improvement of the mechanical properties compared to the mix constituted by sand (~ 80% increase in compressive strength and ~ 180% increase in flexural strength). Hajimohammadi et al. (2018) studied the possibility to use waste glass particles (WGPs) as replacement of river sand in GPC obtained from the alkali activation of FA and GBFS precursors. The higher alkalinity level, introduced by WGPs into the system, promoted the dissolution and reaction in the vicinity of the aggregates, resulting in a denser and stronger

matrix. WGP-based geopolymer mixes were also investigated by Xiao et al. (2020b) as a sustainable pavement base material for road pavement applications.

In this direction, many past and recent studies focused on the optimization of Portland-based mixtures with ground tire rubber (GTR) from automotive end-of-life tires (Roychand et al., 2020; Thomas and Gupta, 2016; Huang et al., 2004). From them, a consensus emerged regarding the peculiarities that the polymer fraction can confer at the concrete materials: lightweight, mechanical toughness, thermo-acoustic insulation, and physico-chemical durability. Such characteristics make the rubberized concrete highly attractive for numerous applications, such as lightweight hollow/solid blocks, shock-wave absorber components, anti-noise barriers, false facades, and paving members (Anwar Khitab et al., 2017). Furthermore, it is well accepted that this approach has promising benefits in terms of environmental and economic impact, i.e., less exploitation of natural resources and "clean"/cheap disposal of waste tires. However, the low mechanical strength in rubberized materials has always represented an obstacle to their large-scale diffusion in the construction industry. Recently, this research topic has also extended to geopolymer matrixes. Aly et al. (2019) investigated the effect of different percentages of GTR as a partial substitution of both fine and coarse aggregates by volume percentage (0, 10, 20 and 30%) on the hardened properties and impact strength of slag based geopolymer concrete, proponing such mixes for structural applications where ductility and resistance to dynamic load are primary requirements (airport runways, bridge approach slabs, railways buffers. Wongsa et al. (2018) studied lightweight geopolymer mortars containing 100 w/w% of 0-4 mm GTR with improved thermal insulation performance (heat conductivity reduction close to 80% than the control mix), which were highly suitable for manufacture of precast components (bricks/blocks) having superior insulating properties. Dong et al. (2021) analyzed the effect of chip rubber particles (2-5 mm and 5-7 mm size gradations) on workability, strength, and durability (carbonation and absorption) properties of FA-GGBS geopolymer concrete, verifying that the compressive strength of rubberized mixes had a strong correlation with bulk density, elastic modulus, ductility, splitting tensile strength and water absorption. Besides, the use of the alkaline activator for both rubber treatment and binder activation did not have a significant impact on the mechanical properties compared to conventional compatibilizing treatments. Lazorenko et al. (2021) implemented a novel chemical pre-treatment of GTR with Potassium permanganate ($KMnO_4$) solution to improve the adhesion properties of the polymer fraction with the geopolymer matrix. As a result of oxidative reactions with $KMnO_4$, polar functional groups are formed on the surface of rubber particles and the surface energy increased, causing a 2.2-fold increment in the hydrophilicity of CR and consequent improvement in rubber-geopolymer binding and mechanical strength (about 21% increase compared to untreated rubberized composite).

However, the number of contributions is still limited for a comprehensive analysis of the influence of GTR on the physical, microstructural, and mechanical behaviour of the material. Building on the previously reviewed literature, expanding the background and knowledge on the use of waste tire rubber as an aggregate in AAM-based matrices would provide a valuable contribution in the field of sustainable construction, directing studies towards more eco-friendly concrete materials (low-carbon binder + recycled fractions in the mix design) with improved functionality for specific applications (lightweight, mechanical toughness, thermo-acoustic insulation, durability). The present work investigated the potential use of GTR to develop geopolymer mixtures containing FA, GBFS and silica fume (SF) as precursors (binder) and sodium hydroxide (NaOH) and sodium silicate ($Na_2SiO_3$) as activators. One of the main objectives of this research was to evaluate the influence of rubber size gradation on the microstructural, physical, and mechanical properties of the geopolymer mixtures. Two rubber fractions, from mechanical grinding of end-of-life tires, were studied in partial/total replacement of natural aggregates: 0-1 mm rubber fine aggregate (in this study referred as RP) and 1-3 rubber granules (RG). A series of tests and analysis, including density, porosity, water absorption, compressive and flexural tests, scanning electron microscopy (SEM), and energy dispersive X-ray analysis (EDX) were conducted for a comprehensive assessment. For comparison purposes, OPC mortars, obtained with the same sand-GTR proportions, were developed, and investigated to rigorously evaluate the advantages and limitations of rubber incorporation in various cementitious composites. Finally, embodied carbon emissions

and cost analysis are also estimated to compare the performance of the two matrices (AAM and OPC), in terms of sustainability and economic impact, following the addition of GTR as aggregate fraction. The incorporation of rubber aggregates in both binder systems (i.e., OPC-based and alkali-activated cementitious composites) has been investigated separately in previous works. However, the inconsistencies in the characteristics of different types of rubber aggregate make any meaningful comparison of results difficult. This study seeks to compare both binder systems employing the same type of recycled rubber aggregates. To the best of the authors' knowledge, no research has adequately compared both binder systems, and this work would be a valuable source for understanding both systems' behaviour.

## 2. Materials and Methods

### *2.1 Raw materials analysis*

Ground tire rubber (GTR) aggregates were supplied from the European Tyre Recycling Association (ETRA, Brussels, Belgium). Two rubber fractions were obtained by ambient mechanical grinding of scrap tires: RP and RG with a nominal size gradation of 0-1 mm and 1-3 mm, respectively. The unit weight, evaluated by an AccuPyc 1330 He-Pycnometer (Micromeritics, Norcross, GA, USA), was 1202 kg/m$^3$. The particle size distribution of rubber aggregates was determined by vibrating sieving analysis using a sieve shaker Giuliani IG/3 (Giuliani Tecnologie, Turin, Italy), in accordance with the specifications reported in ADOT method (2018). Considering the nominal dimension of the two rubber fractions, a specific amount of material and a set of sieves (Retsch, Haan, Germany) were used. Sieves with 0.125 mm, 0.425 mm, 0.710 mm, and 1 mm mesh size were used to analyze RP (70 g). Coarse rubber fraction (280 g) was tested by using mesh sizes of 3 mm, 2 mm, 1.7 mm, and 1 mm. A sampling time of 10/12 minutes was considered for each sieve. The particle size distributions of GTR are given in Figure 1.

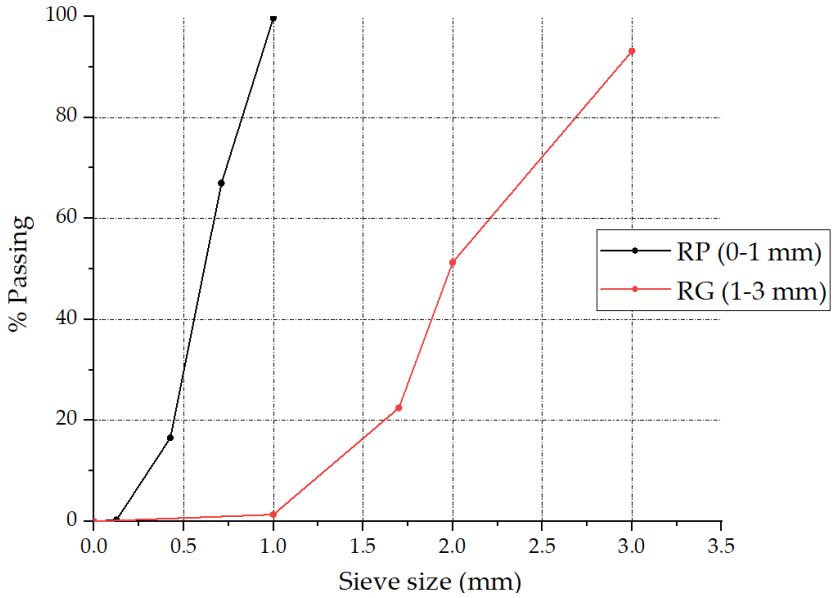


**Figure 1.** Particle size distribution of GTR aggregates.

SEM and EDX were used to evaluate the elemental composition and microstructure of the waste rubber tire particles. SEM micrographs in Figure 3, acquired by Mira 3 FEG-SEM (Tescan, Brno, Czech Republic) in secondary electron (SE) mode, highlights slight differences in morphology between the fine and coarse polymer fraction. RP (Figure 2a) has a more indented and irregular surface texture. On the other hand, RG (Figure 2b) appears smoother and more regular, not presenting rupture zones clearly identified in RP. This

difference is attributable to the different number of grinding cycles required to obtain the two grain sizes distribution: greater particle finesse implies a more irregular final texture. Consequently, a greater specific surface will promote a more effective adhesion of the cement paste with the rubber aggregates (Valente et al., 2020). EDX spectrum (Figure 3), collected by Octane Elect EDS system (Edax, Mahwah, NJ, USA), indicates the obvious presence of Carbon (C) and some secondary chemical elements, Silicon (Si), Sulphur (S), and Zinc (Zn) deriving from fillers typically used in the tire compounds. Specifically, Zn derives from Zinc stearate, a chemical admixture employed as activator in the rubber vulcanization process (Wik and Dave, 2009). Zinc stearate contributes to the poor rubber-cement interface adhesion. Such compound diffuses to the rubber surface, creating a hydrophobic coating that hinder the binding with the cement paste (Youssf et al., 2016).

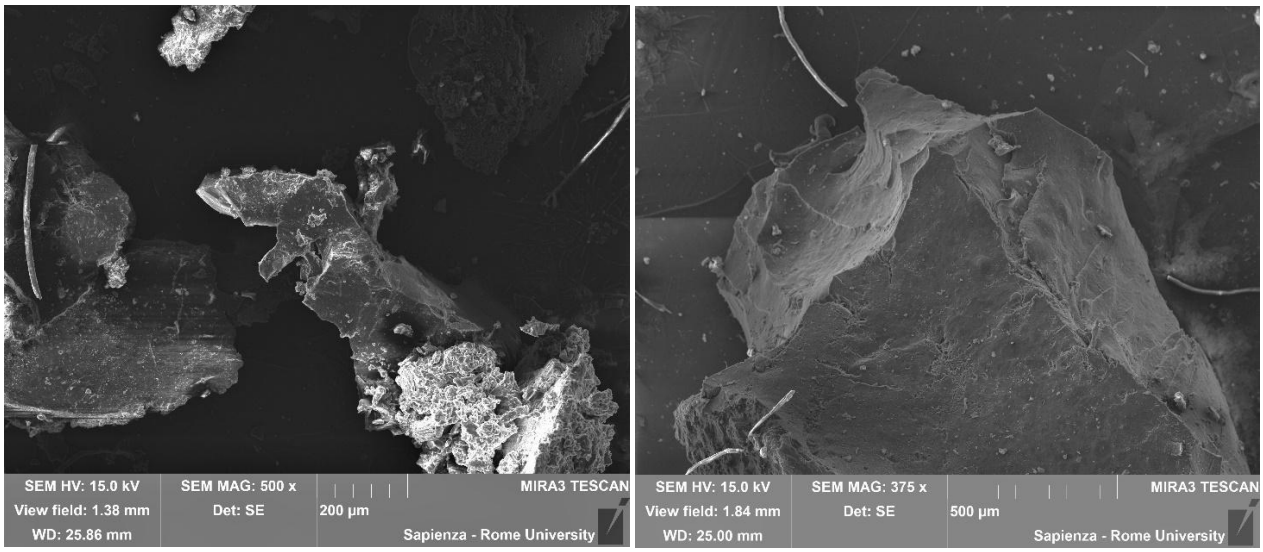


(a) (b)

**Figure 2.** SEM microstructural analysis on GTR aggregates: RP (a) and RG (b).

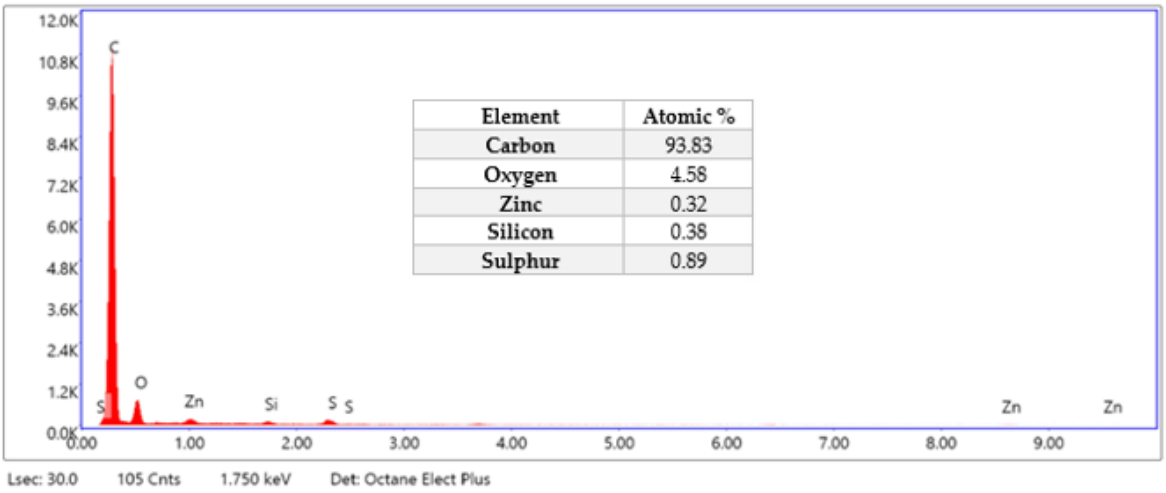


| Element | Atomic % |
|---|---|
| Carbon | 93.83 |
| Oxygen | 4.58 |
| Zinc | 0.32 |
| Silicon | 0.38 |
| Sulphur | 0.89 |

**Figure 3.** EDX analysis on GTR aggregates. Atomic composition data are average values of six EDX measurements.

Type I Portland cement was used as a binder for the OPC-based formulations. Limestone sand of size 0-0.4 mm was used as natural aggregates and sourced from an Italian supplier. A specific blend of chemical admixtures in powder form (SIKA, Zurich, Swiss), including silica fume thixotropic agent, poly-carboxylic ether polymer-based superplasticizer, aliphatic-based water reducing additive, and Calcium oxide-based

expansive agent, was used to optimize the rheology of the fresh mixture. Detailed information on the admixtures can be found in a past work (Sambucci et al., 2020). Common tap water was used for the hydration of the cement mixes.

Based on some of the authors' previous works, three low-carbon binder materials were employed to prepare the Alkali Activated Materials (AAM). Fly Ash (FA), supplied by Cemex (Cemex, Rugby, UK), was used following BS EN 450-1 (2012). Ground Granulated Blast-Furnace Slag (GGBS) used in this study was provided by Hanson (Hanson, Maidenhead, UK). Ultra-fine Silica Fume Sand (SF) grade 0.06 – 0.3 mm was obtained from SIKA (SIKA, Zurich, Swiss). The characterisation of each binder material can be found in our previous studies (Chougan et al., 2020; Albar et al., 2020; Chougan et al., 2021). Sand was sieved in accordance with BS EN 410-1 (2000) to achieve particle size ranges of 0-0.5mm and 0.5-1.0 mm. Alkaline activators used for making the AAMs consisted of alkali silicate and hydroxide solutions. The alkali silicate was Sodium silicate ($Na_2SiO_3$), supplied by Solvay (Vila Franca de Xira, Portugal), having a $SiO_2/Na_2O$: 3.23 (8.60 wt% $Na_2O$, 27.79 wt% $SiO_2$, 63.19 wt% $H_2O$, 0.4 wt% $Al_2O_3$). A 10 M sodium hydroxide solution was provided by dissolving sodium hydroxide (NaOH) pellets with 98% purity (Fisher Scientific, Germany) in deionized water and cooled before use. The alkali solution was performed by mixing NaOH and $Na_2SiO_3$ (1:2 ratio) separately for 5 minutes at 700 rpm using a 230V/50Hz magnetic stirrer (Fisher Scientific, Loughborough, UK).

The raw materials of Portland and geopolymer mixes (limestone sand, SF, FA, and GGBS) were analyzed by powder X-ray diffraction (XRD), employing a D8 advanced Bruker AXS diffractometer (Bruker, Millerica, MA, USA), Cu-K$\alpha$ radiation, wavelength of 1.542 Å, and beam radiation set to 40 kV and 40 mA. XRD patterns of limestone sand and SF (Fig. 4a-b) indicate the presence of Quartzite as the major phase and secondary signals deriving from Calcite. The sharpness of the peaks reveals the high crystallinity of these mineral components. Quartzite and Calcite crystalline phases are also identifiable in equal distribution in FA (Fig. 4c), where it is possible to observe the coexistence of Mullite. XRD pattern of GGBS (Fig. 4d) highlights its highly amorphous structure, resulting from a high percentage of glass phase (about 90%). The minor phases of crystalline nature detected were Diopside and Gehlenite.

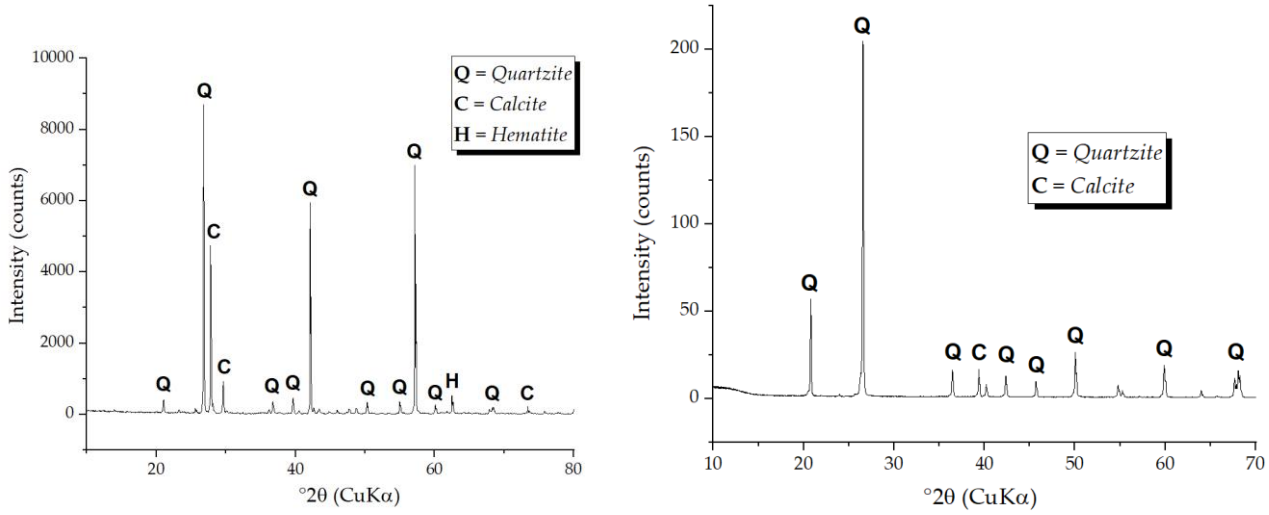


(a) (b)

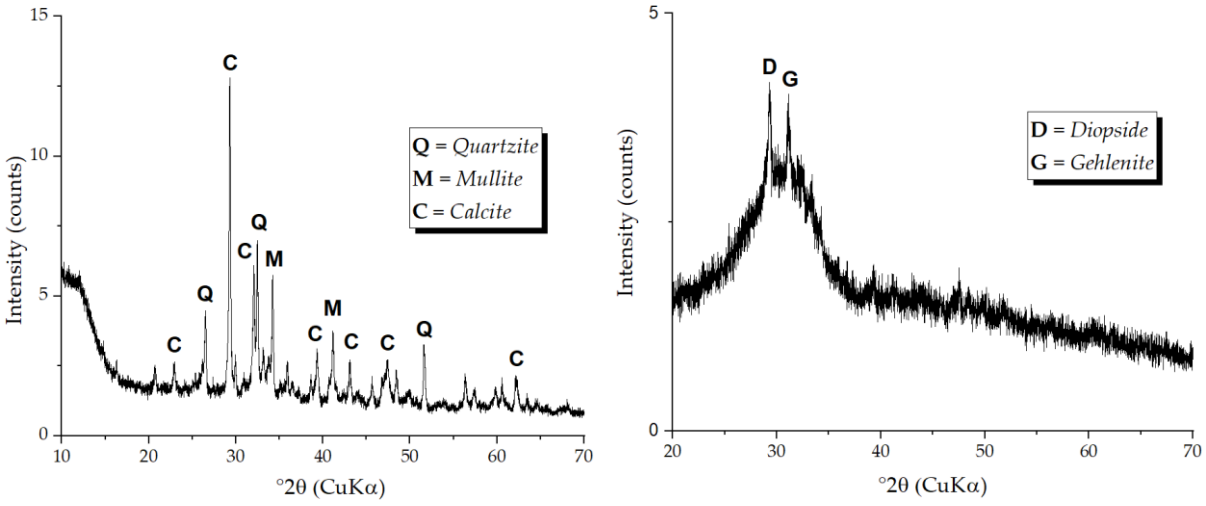


**Figure 4.** XRD pattern of limestone sand (a), SF (b), FA (c), and GGBS (d).

### *2.2 Mixture proportions and samples manufacturing: OPC mixes*

The replacement of limestone sand from GTR is used to prepare cementitious mixes at different volumetric percentages of 0% (Control mix), 50%, and 100%. In total four rubber-cement formulations were developed, varying the proportion ratio of RP and RG and the water dosage (Table 1). After mixing the dry components for 45 s, water was incorporated in the batch and further mixing was performed for 12 min. The fresh paste was then poured into steel formwork to produce 40 mm x 40 mm x 160 mm beams. After 28-days of ambient curing (at 20°C), the beams were demoulded and tested in flexural. 40-mm side cubic specimens were extracted, by cutting with a diamond blade saw, from the post-failure samples for compressive test. For porosity and water absorption measurements, 40 x 10 x 10 mm prisms were cut from the beams.

**Table 1.** Mix designs of rubber-OPC formulations.

| Sample | Cement (kg/m³) | Water (kg/m³) | Sand (kg/m³) | RP (kg/m³) | RG (kg/m³) | Admixtures (kg/m³) |
|---|---|---|---|---|---|---|
| **Control-OPC** | 800 | 300 | 1100 *(100 vol.%)* | 0 *(0 vol.%)* | 0 *(0 vol.%)* | 152 |
| **S50-RP50-OPC** | 800 | 280 | 550 *(50 vol.%)* | 150 *(50 vol.%)* | 0 *(0 vol.%)* | 152 |
| **RP100-OPC** | 800 | 260 | 0 *(0 vol.%)* | 300 *(100 vol.%)* | 0 *(0 vol.%)* | 152 |
| **RP50-RG50-OPC** | 800 | 250 | 0 *(0 vol.%)* | 150 *(50 vol.%)* | 160 *(50 vol.%)* | 152 |
| **RP25-RG75-OPC** | 800 | 230 | 0 *(0 vol.%)* | 75 *(25 vol.%)* | 240 *(75 vol.%)* | 152 |

### *2.3 Mixture proportions and samples manufacturing: AAM mixes*

The replacement (by volume) of sand from GTR is used to prepare AAM mixes like that of OPC-based mixtures (i.e., 0 vol.%, 50 vol.%, and vol. 100%). All the solid components including binder (i.e., FA, GGBS, and silica fume), and aggregates (graded sand and GRT), were mixed in dry condition for 2 minutes at 250rpm using a planetary mixer (Kenwood, Havant, UK) to homogenise the dry mixture. The activator solution was gradually added to the dry mix. The mixing process continued until a homogeneous mixture was obtained.

For the casted samples, fresh mixes poured into prismatic moulds with dimensions of 40mm x 40mm x 160mm. To ensure initial hydration would occur as well as effective alkali activation, the moulds were then wrapped in plastic and placed in an oven at 60°C for 24 hours. Finally, the samples were removed from the oven and allowed to cure for 6 days at room temperature. Testing samples were extracted similarly to OPC-ones. Table 2 shows the mix designs of five AAM mixtures, varying the proportion ratio of RP and RG. All the geopolymer mixes were prepared with a constant water/solid ratio of 0.4.

**Table 2.** Mix designs of rubber-geopolymer formulations.

| Sample | Binder (wt.%) | | | Aggregate (vol.%) | | | $Na_2SiO_3$:NaOH (by mass) | Activator/Binder (by mass) |
|---|---|---|---|---|---|---|---|---|
| | FA | GGBS | SF | Graded sand* | RP | RG | | |
| **Control-AAM** | 60 | 25 | 15 | 100 | 0 | 0 | 2:1 | 0.4 |
| **S50-RP50-AAM** | 60 | 25 | 15 | 50 | 50 | 0 | 2:1 | 0.4 |
| **RP100-AAM** | 60 | 25 | 15 | 0 | 100 | 0 | 2:1 | 0.4 |
| **RP50-RG50-AAM** | 60 | 25 | 15 | 0 | 50 | 50 | 2:1 | 0.4 |
| **RP25-RG75-AAM** | 60 | 25 | 15 | 0 | 25 | 75 | 2:1 | 0.4 |

** Graded sand contains 60 Wt. % of size 0-0.5mm and 40 Wt. % of size 0.5-1.0mm.*

By way of comparison, Figure 5 shows the surface textures of geopolymer and OPC samples after curing.

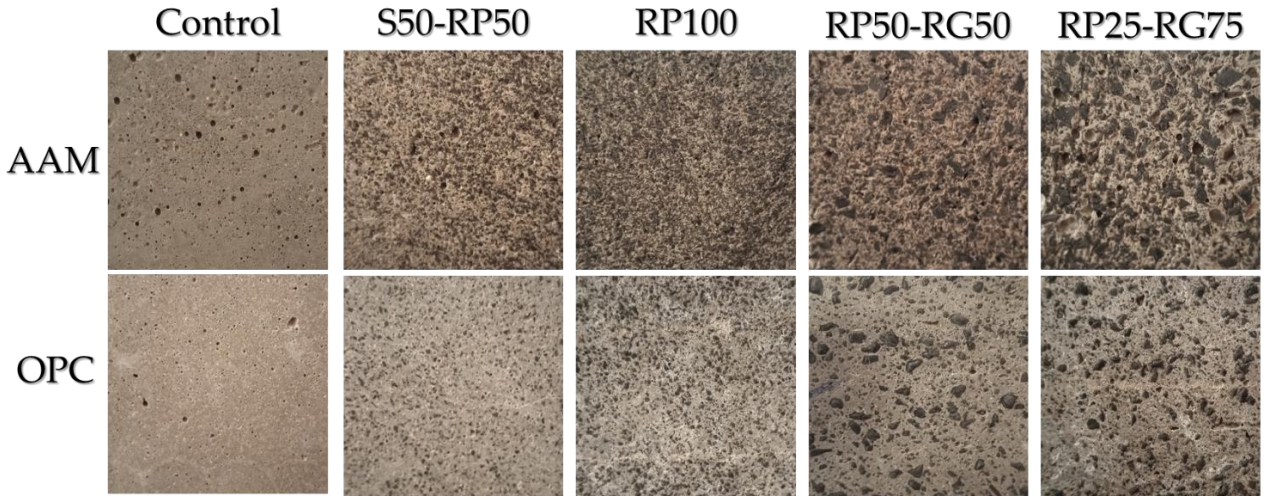


**Figure 5.** Comparison of the surface texture between AAM and OPC mixes.

### *2.4 Testing*

#### *2.4.1. SEM and EDX analysis*

Microstructural properties of Portland and geopolymer samples were investigated using a Mira 3 FEG-SEM (Tescan, Brno, Czech Republic). Fracture surfaces of the specimens were sputter-coated with graphite to make the material conductive for the analysis. This pre-treatment was performed by an EM SCD005 vacuum sputter coater (Leica, Wetzlar, Germany).

Octane Elect EDS detector (Edax, Mahwah, NJ, USA), attached to SEM, was employed to determine the influence of GTR addition on the elemental composition of Portland and geopolymer binders. The analysis provided elemental mapping results of the AAM matrices, acquired at an accelerating voltage of 15 kV, verifying the variation of the fundamental elemental ratio (Si/Al ratio) as a function of the incorporation of rubber in replacement of the mineral aggregates. Furthermore, this technique was used to compare the

elemental composition of the polymer aggregates integrated into the two binders, to provide support to the experimental results on the OPC-GTR and AAM-GTR interface properties.

*2.4.2. ATR-FTIR chemical analysis*

The Attenuated Total Reflectance in conjunction with Infrared Spectroscopy (ATR-FTIR) measurements were performed to study functional groups at the surface of GTR prior and after incorporation into the two matrices (OPC and AAM). The rubber particles were carefully removed from hardened mortars and analyzed with a PerkinElmer Spectrum 3 FT-IR spectrometer (PerkinElmer, Waltham, MA, USA). The samples were deposited on the attenuated total reflectance ZnSe crystal plate using a top-plate and pressure-arm accessories. A force of 12 N was applied to allow a proper contact of the rubber with the diamond crystal. The resolution in the spectra was 4 $cm^{-1}$ and 4 scans were run per sample.

*2.4.3. Density evaluation*

Density of hardened samples was calculated by weight and size measurements by means of a digital caliper and a ME54 analytical balance (Mettler Toledo, Columbus, OH, USA). For each formulation under examination, four samples were investigated, and the average value of the density measurements was reported.

*2.4.4. Porosity and water absorption measurements*

Permeable porosity (φ) and water absorption (WA) were determined using vacuum saturation method, conforming to ASTM C1202 (2002). The specimens were first oven dried (105°C for 24 h) and then weighted ($W_d$). The dry samples were put in a glass vacuum desiccator connected to a Divac 0.6L diaphragm pump (Leybold, Cologne, Germany). The pumping system was activated to evacuate moisture within the material and operate under vacuum conditions of about 40 mbar for 30 min. Then the desiccator was filled with tap water, keeping the samples immersed for another 30 min. Finally, the pumping system was deactivated, and the specimens were left under water for 3 h. By configuring the analytical balance to perform weight measurements using the hydrostatic method, the mass of the specimens immersed in water ($W_w$) and the mass of the saturated specimens in air ($W_s$) were recorded. The average values of φ and WA, obtained from four samples, were computed using the following equations (1-2):

$$\varphi = \frac{W_s - W_d}{W_s - W_w} \times 100 \qquad (1)$$

$$WA = \frac{W_s - W_d}{W_d} \times 100 \qquad (2)$$

*2.4.5. Mechanical tests: Compressive and flexural tests*

Compressive test was conducted for hardened cubic specimens following the requirements of ASTM C109/C109M-20a (2020) standard method. The experimentation was performed by a 150 kN universal testing machine (Zwick-Roell Z150, Ulm, Germany) at a loading rate of 1 mm/min. Three-point flexural test was conducted on beam samples using a Zwick-Roell Z10 apparatus (load cell of 10 kN, loading rate of 1 mm/min, and span distance of 100 mm) in accordance with ASTM C348 standard test method (2020). The stress–deformation curves and the mechanical properties were recorded using TestXpert testing software. The results of compressive and flexural tests are the average of values obtained from three specimens. To corroborate the mechanical results, some post-fracture micrographs were collected using a MS5 stereomicroscope (Leica, Wetzlar, Germany).

***2.5 $ECO_2$ emissions and cost analysis***

This section provides an estimation for the embodied $CO_2$ ($ECO_2$) and cost analysis (CA) of the concrete mixes developed in this work, to assess the environmental and economic impact resulting from the substitution of GTR with the natural aggregates in the two matrices (OPC and AAM) under investigation. As a preliminary evaluation, Control mixes were compared with RP100 formulations, having the highest content of rubber at the same sand-GTR replacement level. The evaluation follows the calculation model proposed by Bostanci et al. (2018), which includes in the computation the "cradle-to-factory gate" (or product stage) emissions (raw materials supply + manufacturing). According to Equations 3 and 4, $ECO_2$ emissions ($ECO_2$), in kg CO2/ton, and overall cost, in €/ton, of concrete mix designs were computed by multiplying the mass (m) of each ingredient (refer to 1 ton of mix) by its $ECO_2$ coefficient (EC), in $kgCO_2/kg$, and price (P), in €/kg, respectively.

$$ECO_2 = \Sigma\, m_i \times EC_i \quad (3)$$

$$CA = \Sigma\, m_i \times P_i \quad (4)$$

where "i" refers to the i-esimal component of the mix design.

Regarding the OPC-based formulations (manufactured in Sapienza University of Rome labs), EC and P values of source materials (Type I Portland cement and limestone sand) were obtained from the Italian Environmental Product Declaration (EPDItaly) database, which collects environmental compliance declarations from the main local manufacturers of building and construction materials. Average data about the eco-profile, in terms of $CO_2$ emissions, of chemical admixtures was extrapolated from the Environmental Declaration Superplasticizing Admixtures, provided by European Federation of Concrete Admixtures Associations (EFCA). The market cost of the admixture blend was estimated by SIKA manufacturer. The eco-impact deriving from the use of mixing water was also included in the analysis, taken from the life cycle assessment (LCA) study conducted by Botto (2009). Water consumption costs were agreed to the Italian tariff for industrial use.

Regarding the AAM-based formulations (manufactured in Brunel University of London, AMTC research group), EC and P values of aluminosilicate binders and natural aggregate (FA, GGBS, SF, and sand) were deduced from (Bostanci et al., 2018), in agreement with Mineral Product Association (MPA), which is the trade body for the UK's aggregates, cement, and concrete industries. EC values of alkali activators ($Na_2SiO_3$ and NaOH) were referred to the LCA study on geopolymer mixes edited by Dal Pozzo et al. (2019) and their average P indices were taken by (Petrillo et al., 2016).

Regarding GTR, an indicative EC value, deriving from electricity consumption for ambient grinding treatment, was obtained from (Rashid et al., 2019). The average cost of polymer aggregates was provided by the supplier (ETRA). A summary of EC and P indicators used for the environmental impact and cost analysis is reported in Table 3.

**Table 3.** EC and P indicators of OPC and AAM mix designs for cost-emissions analysis.

| **OPC mixes** | | |
|---|---|---|
| **Constituent** | **EC ($kgCO_2/kg$)** | **P (€/kg)** |
| Type I Portland cement | 0.788 | 0.198 |
| Limestone sand | 0.021 | 0.092 |
| Chemical admixtures | 0.690 | 0.100 |
| Water | 0.001 | 0.001 |
| **AAM mixes** | | |
| **Constituent** | **EC ($kgCO_2/kg$)** | **P (€/kg)** |
| FA | 0.004 | 0.178 |
| GGBS | 0.067 | 0.130 |
| SF | 0.014 | 0.237 |
| Sand | 0.005 | 0.038 |
| $Na_2SiO_3$ | 1.222 | 0.600 |

| | | |
|---|---|---|
| NaOH | 1.915 | 0.300 |
| **GTR** | | |
| **Type of fraction** | **EC (kgCO2/kg)** | **P (€/kg)** |
| RP | 0.004 | 0.158 |

# 3. Results and discussions

## *3.1 SEM and EDX analysis*

For an effective discussion of the physical-mechanical features of the rubberized formulations developed in this research work, it is necessary to report first a comparison in terms of microstructure and GTR-matrix interface properties between geopolymer and OPC binders.

### *3.1.1. SEM comparative analysis: Control samples*

Figure 6 reports a comparison between OPC and geopolymer Control microstructures (0% GTR) by SE micrographs. Notable differences can be observed between the two matrices. OPC microstructure (Fig.6a) presents the typical calcium-silicate-hydrate (C-S-H) phase (tag "A") which appears quite homogeneous. Besides, it is possible to identify some air bubbles (tag "B") that remain inadvertently trapped in the material during the mixing of the fresh paste. Finally, a good cohesion between the mineral aggregate (tag "C") and the OPC binder can be detected. High magnification SEM image (Fig.6b) reveals lamella-shaped Portlandite (C-H) crystals into the cement phase. On the other hand, geopolymer microstructure appears much more heterogeneous. As shown in Figure 6c, the matrix involved the coexistence of uniform aluminosilicate phase (tag "A¹"), due to the proper occurrence of precursor activation and microstructural development, more unreacted FA particles (tag "B¹"), and spheroidal cavities and pores (dashed circles), resulting from several aspects: a) hollow spaces left behind by dissolved FAs; b) partially dissolution of FA particles that create porosity in the matrix; c) air entrained during the mixture preparation. The sand aggregate (tag "C¹") seems to intercalate correctly with the matrix. As demonstrated by previous studies (Kong et al., 2007; Kramar and Ducman, 2015), this is the common microstructural array characterizing geopolymer concretes synthesized by FAs. High-scale micrograph in Figure 6d details that some FA particles experienced activation owing to the effect of the alkaline activator and generated surface reaction products, resulting in rod-shaped crystals. Unreacted particles were recognized by the neat and morphologically unaltered surface.

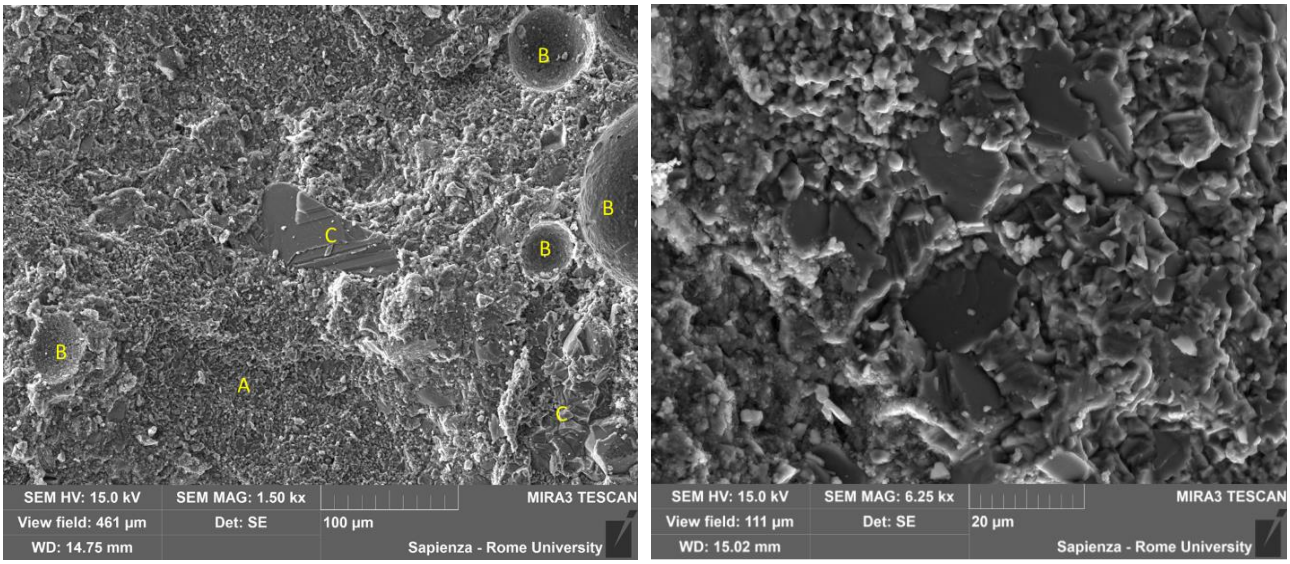


**(a)** **(b)**

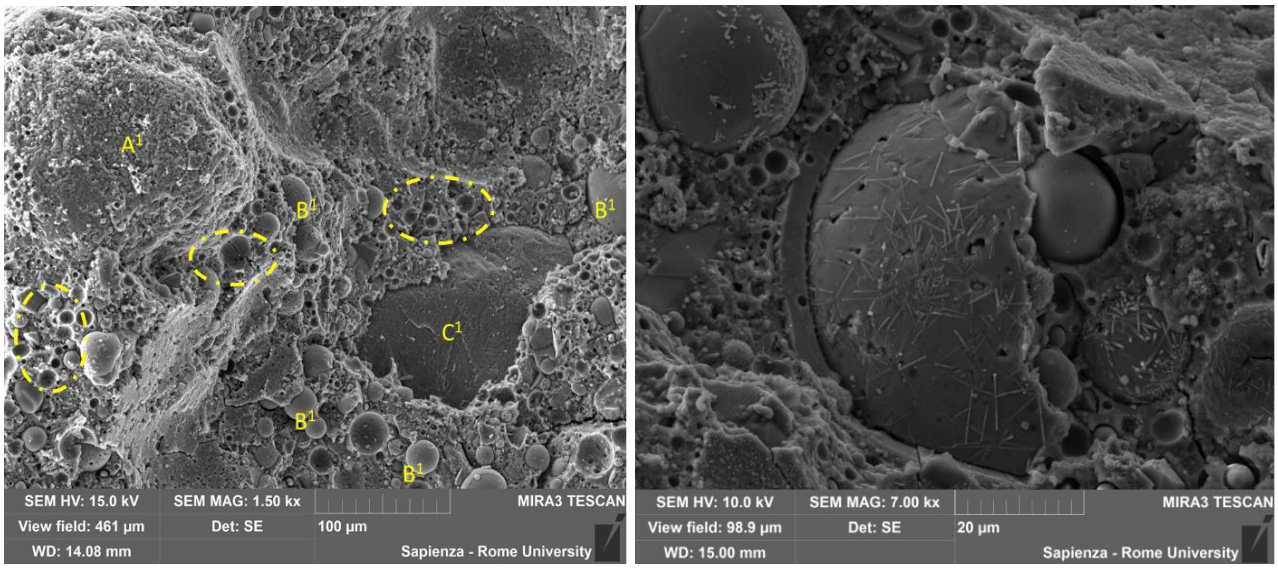


**(c)** **(d)**

**Figure 6.** Comparative analysis by SEM between Control-OPC (a-b) and Control-AAM samples (c-d).

*3.1.2. SEM and EDX comparative analysis: Rubberized samples*

SEM analysis reported below were performed with the purpose of investigating the influence of the type of matrix and the GTR size gradation on the rubber-binder adhesion properties.

Figure 7 compares the rubber-OPC interface properties in the case of RP (Fig. 7a) and RG (Fig. 7b). As previously mentioned in Section 2.1, the finest rubber fraction provided a "jagged" morphology, which is characterized by structural indentures where the cement paste can penetrate and anchor with the polymer particle. Conversely, the coarse fraction exhibits a smooth texture which hinders the cohesion of the matrix, highlighting a more evident interfacial discontinuity. Therefore, in the case of GTR-OPC bond, the adhesion properties are mainly governed by physical interaction between polymer and matrix. Interface porosity is however detectable due to the chemical mismatch between rubber and the cementitious binder (i.e., Zinc stearate effect).

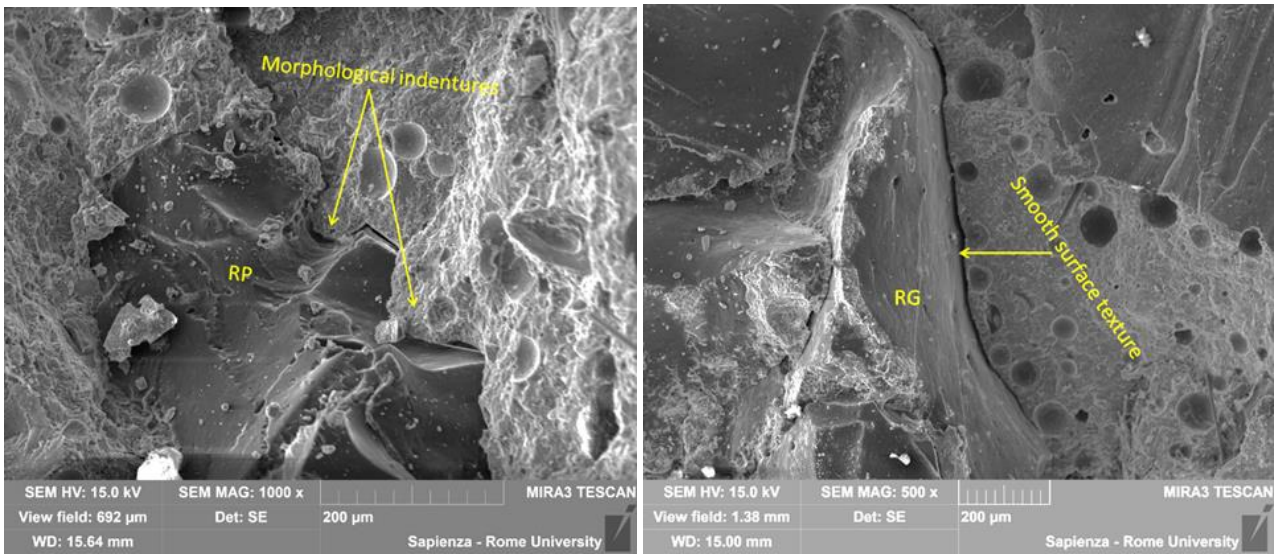


**(a)** **(b)**

**Figure 7.** Rubber-OPC interface properties: RP (a) and RG (b).

Figure 8 below reports a similar analysis but considering GTR-geopolymer adhesion. Figures 8a and 8b show RP aggregates well integrated into the geopolymer matrix, with no interfacial gaps. The binder adheres continuously and homogeneously to the polymer aggregate, as also clearly visible in the zoomed micrographs. Unlike GTR-OPC interface properties, it is evident that a strong chemical interaction is established between the polymer particles and the geopolymer, which is directly attributable to the mix design of the alkali-activated composites. The synthesis of geopolymer mortars proposed in this research involves two components extensively studied as compatibilized agents to improve rubber-cement cohesion: NaOH and SF. Li et al. (2019a) reviewed the effect of these treatments on the potential enhancement of the GTR-cement compatibility. Improvement in the performance of rubberized concrete via NaOH pretreatment is related to three reasons: a) the alkaline solution removes impurities from the surface of the particles promoting the bond with the cement matrix; b) NaOH increases the surface roughness of the polymer aggregates; c) the adverse influence of Zinc stearate is inhibited upon conversion to a water-soluble product (Sodium stearate) which is removed from the rubber surface. Due to its high pozzolanic reactivity, SF acts as a coupling agent, increasing the rubber hydrophilicity, and enhancing the establishment of chemical bonds with the cement matrix. Besides, it performs a filling effect for nanometric voids, including the interface gaps between rubber aggregates and cement matrix, leading to a denser microstructure (Xie et al., 2019). Although the SF is also used in Portland mixtures, it is part of the admixture blend and is entirely involved and consumed in the hydration reaction of the cement paste. SF particles undergo rapid dissolution in the calcium hydroxide solution, forming a Ca-poor Si-rich phase that acts as a substrate for the formation of conventional CSH gel (Langan et al., 2002). Conversely, in the AAM-based mixes SF fraction composes the binder blend, and its availability could be sufficient to also assist the GTR-geopolymer compatibilization.

Figure 8c shows the RG-geopolymer interface properties, highlighting the co-presence between a good rubber-matrix bond (detailed in Figure 8d), in accordance with the chemical compatibility previously discussed, and weak adhesion, due to the incongruous morphology of the coarse fraction. Figure 8d also elucidates the role of rubber aggregates on the mechanical behavior of the material. It is noted how the elastic nature of the polymer blocks the crack propagation, delaying its coalescence and consequently promoting the toughness of the mortar and its pre-failure deflection properties (Guo et al., 2019).

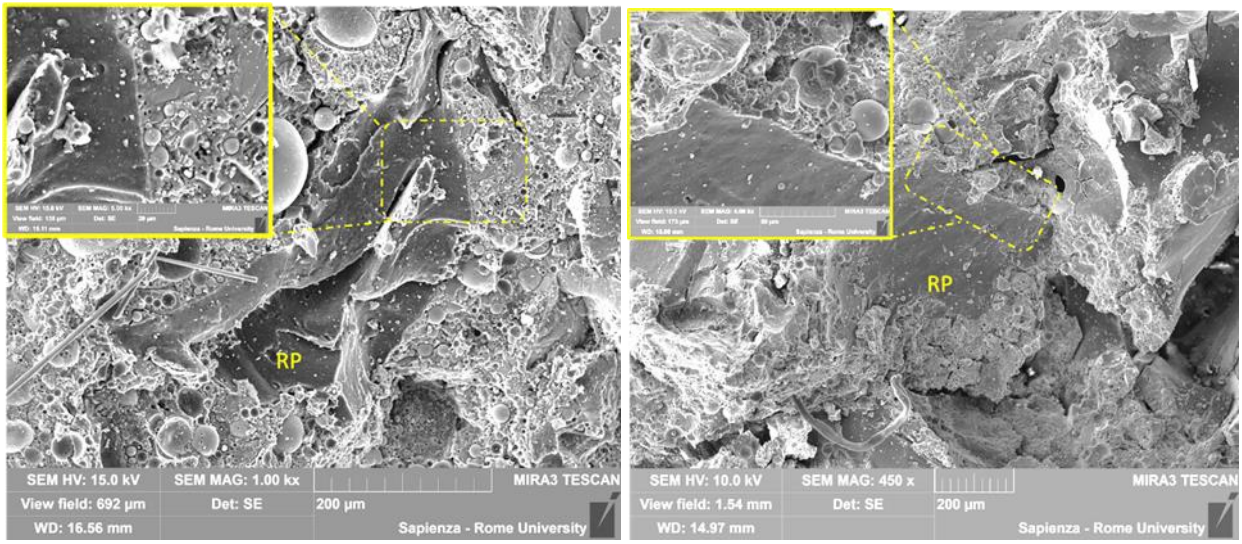


**(a)** **(b)**

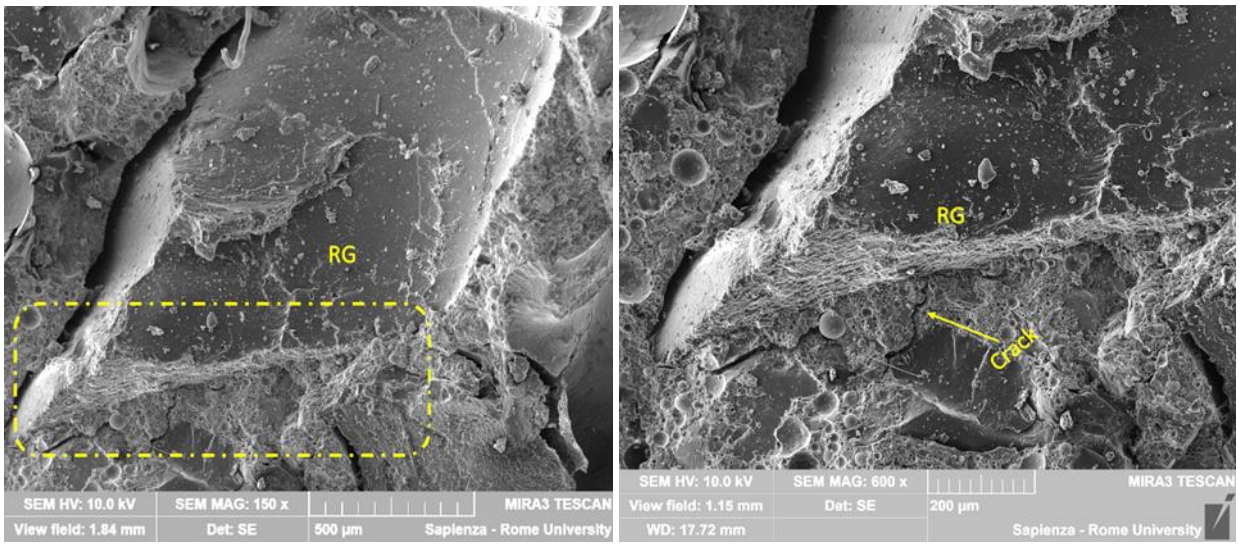


**(c)** **(d)**

**Figure 8.** Rubber-Geopolymer interface properties: RP (a-b) and RG (c-d).

To consolidate the argument regarding the influence of the NaOH-based alkaline activator on the greater compatibility of rubber aggregates with the geopolymer matrix compared to the OPC one, Figure 8 shows a comparison between the EDX spectra of the GTR surface in the case of incorporation into the Portland cement (Figure 9a) and in AAM binder (Figure 9b). In the geopolymer matrix, the elemental composition of GTR is free from the Zn-signal and highlights the Na-band, which is probably derived from Sodium stearate. Differently, Zn-signal remains unchanged in the spectrum inherent of Portland-based sample. This difference is potentially indicative of the removal of Zinc stearate from rubber by NaOH solution during the processing of geopolymer mixes, positively affecting rubber-matrix cohesion in AAM mixes.

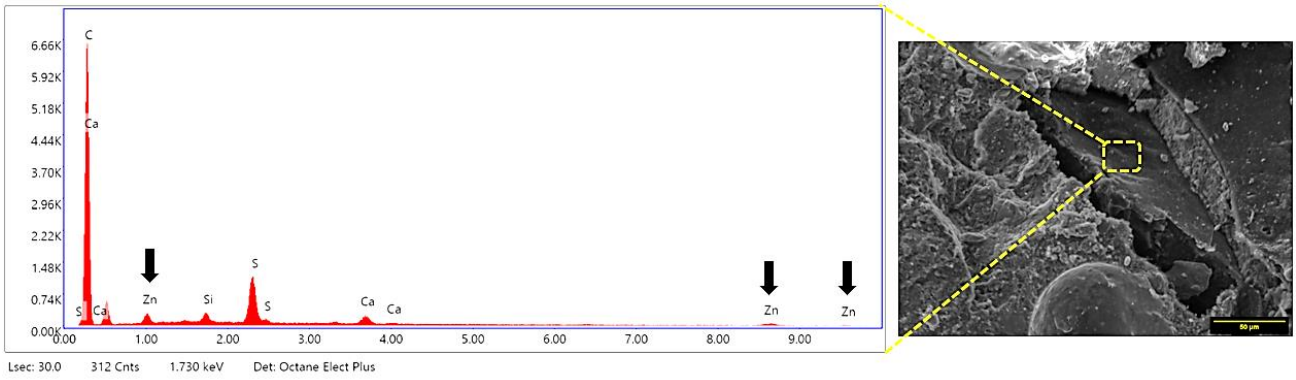


**(a)**

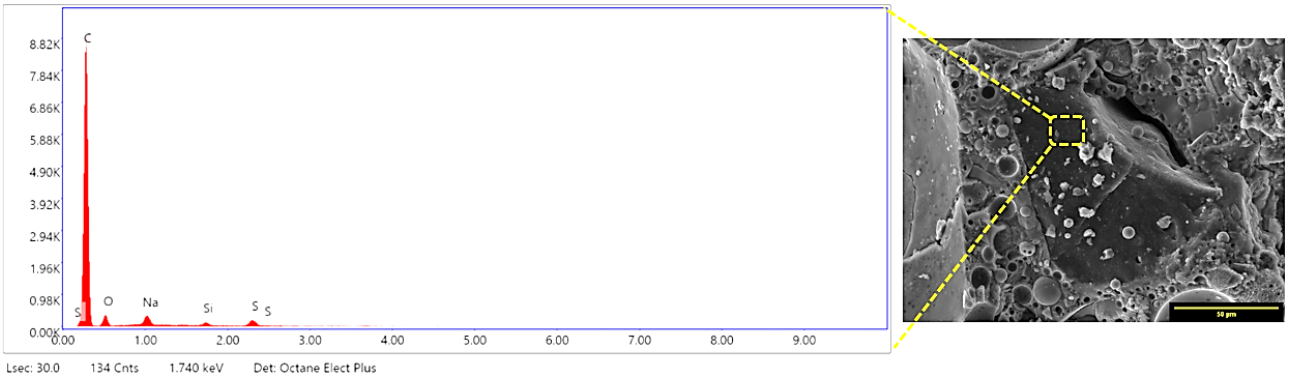


**(b)**

**Figure 9.** EDX spectra of GTR in Portland (a) and AAM (b) matrices

### *3.2. ATR-FTIR chemical analysis*

ATR-FTIR technique was implemented to evaluate any variations in the surface chemical composition of the rubber aggregates in case of incorporation into the two binders (OPC and AAM) and to verify, in support of the EDX analysis, whether the AAM mix design is able to "clean up" the polymeric particles from Zinc stearate, promoting their compatibility with the matrix. ATR-FTIR absorbance spectra of crude GTR particles and after extraction from OPC and AAM matrices are compared in Figure 10a. The peaks at 2915 $cm^{-1}$ and 2846 $cm^{-1}$ (*Zone 1*) are ascribed to typical C − H stretching vibrations (asymmetrical and symmetrical stretching, respectively) of $CH_2$ groups present in the aliphatic chains of the elastomer (Lanzón et al., 2015). *Zone 3* shows some absorption peaks below 1000 $cm^{-1}$ that do not appear in the crude rubber sample. These could be attributable to a small amount of binder paste (both OPC and AAM) remaining partially adhered to the rubber surface after removal. C-S-H vibration for OPC (Parande et al., 2011) and Si−O−T (T = Si or Al) asymmetric stretching for AAM (Rees et al., 2007) are the possible assignments of the low-wavenumber signals. *Zone 2* (zoomed in Figure 10b) identifies the molecular vibrations related to Zinc stearate. In crude GTR spectrum, the sharp peak at 1539 $cm^{-1}$ and the weak signal at 1396 $cm^{-1}$ are assigned to the antisymmetric and symmetric vibrations of the carboxylate group (COO), characterizing the molecular structure of the vulcanization activator (Lanzón et al., 2015; Parsaie et al., 2021). After removal from the OPC matrix the polymer aggregate would seem to partially lose the compound probably due to the action of the alkaline environment of the cement paste. However, the permanence of the absorption band at 1373 $cm^{-1}$ would confirm that Zinc stearate was still present on the surface. On the other hand, after exposure in the AAM matrix, it is noted that the characteristic absorption of Zinc stearate disappears from the spectrum, resulting in a flat signal due to the leaching effect by NaOH activator.

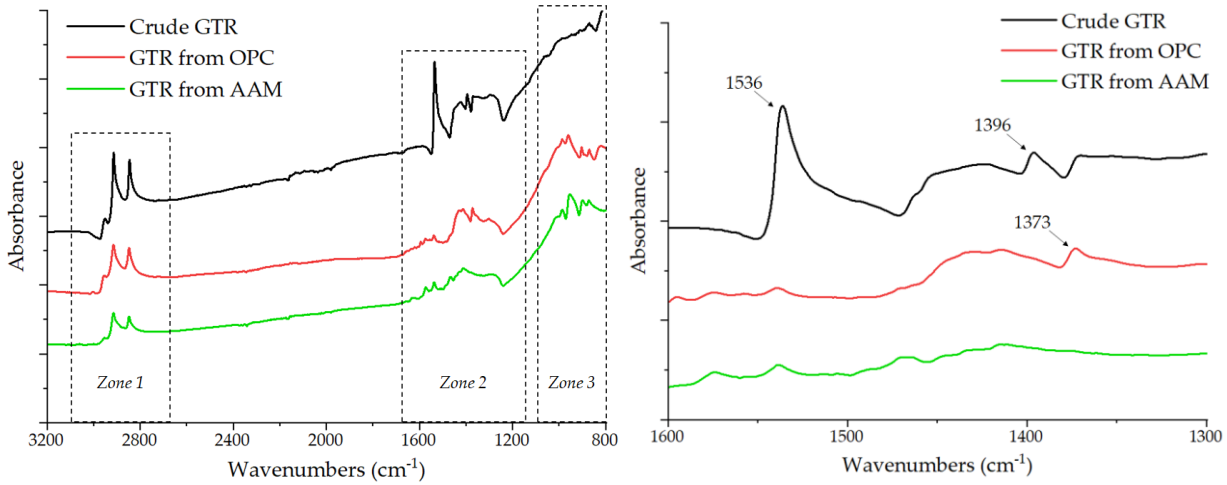


**Figure 10.** (a) ATR-FTIR spectra of crude GTR particles and after extraction from OPC and AAM matrices. (b) Zoomed spectral range related to Zinc stearate signal.

### *3.3. Density evaluation*

The density results for the OPC and geopolymer formulations are given in Figure 11. Using lightweight rubber aggregates to replace sand resulted in an obvious decrease in the unit weight (Roychand et al., 2020; Thomas and Gupta, 2016; Wongsa et al., 2018; Dong et al., 2021). It was observed that the reduction rate is related to the sand-GTR replacement level and, at the same rubber content (i.e., 100 vol.%), to the proportion ratio between fine and coarse polymer fraction. With respect the Control sample, in OPC-based mortars the density decreased by 14.8%, 30.5%, 15.7%, and 23.8% in S50-RP50-OPC, RP100-OPC, RP50-RG50-OPC, and RP25-RG75-OPC mixes, respectively. In the geopolymer composites, the rate drops were 17.7%, 31.2%, 27.6%, and 27% in S50-RP50-AAM, RP100-AAM, RP50-RG50-AAM, and RP25-RG75-AAM mixes, respectively. In both types of binders, the strongest reduction level was found in the RP100 formulations: the presence of only the finest polymer fraction implied a higher rubber content per unit of volume. Indeed, the mixes functionalized with RG recorded a slight gain in density. In OPC-based samples, by increasing RG content a greater unit weight reduction was observed. Conversely, in geopolymer blends the density remained almost constant. This opposite trend can be attributed to the different interface features between rubber and matrix previously observed. Better adhesion found in geopolymer matrices positively impacts on the material densification.

Another salient result concerns the divergence in density percentage drop between OPC and geopolymer mixes. From the experimental data, Portland matrix seems to be less affected by the sand-rubber replacement in terms of unit weight loss, showing lower reduction rates than the geopolymer counterpart. One of the hypotheses eligible for this evidence could be the contribution of the mineral aggregates on proper microstructural development of the geopolymer binder. As reported in literature (Mermerdas et al., 2017), sand acts as Si-source for the geopolymerization, actively contributing to the formation of the aluminosilicate phase. In this regard, Arellano-Aguilar et al. (2014) demonstrated that the densification of the geopolymer gel increased with the Si/Al ratio, as the establishment of more Si-O-Si bonds occurred. Therefore, GTR as alternative aggregates could inhibit this mechanism. To clarify this aspect, EDX analysis, presented later in the manuscript, will investigate the influence of the polymer inclusions on the chemical characteristics of the geopolymer mortars in terms of Si/Al ratio variation.

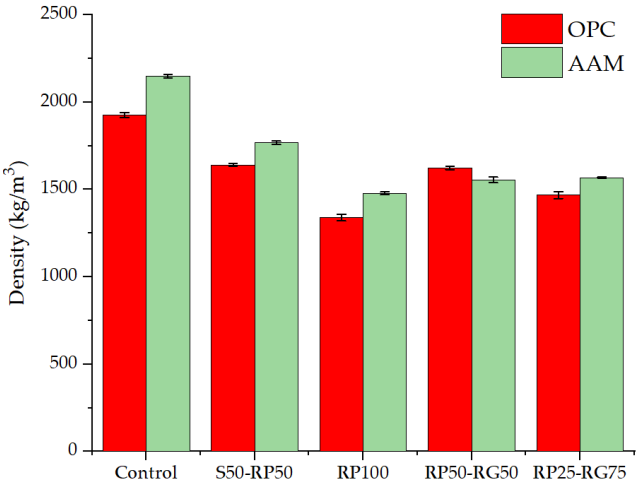


**Figure 11.** Density values of OPC and geopolymer mixes.

### *3.4. Porosity and water absorption measurements*

In this preliminary investigation, porosity and water absorption were considered as durability indicators to evaluate the effect of rubber on the material's performance. The experimental results are reported in Figure 12.

Past studies (Angelin et al., 2017; Girskas and Nagrockienė, 2017; Di Mundo et al., 2019) demonstrated an increase in the effective porosity of concrete modified with tire rubber, mainly resulting from the non-polar nature of the polymer particles which tends to expel water and trap air in the matrix. In addition, the poor adhesion between rubber and cement paste generates microstructural gaps that contribute to the pore structure of the material. In accordance with the experimental results reported in Figure 12a, a slight increase in porosity was recorded in all the OPC-based rubberized mixes, except for the RP100-OPC sample, where a little decrement in φ-value occurred with respect to Control-OPC mix. Although further investigations are needed to understand this trend, in the first hypothesis it is possible to states that the finest fraction could act as a micro-filler to fill up the permeable voids into the concrete matrix, which combined with its non-porous and non-absorbent nature would provide a positive effect on the overall porosity of the material. Similar finding was found by Sukontasukkul and Tiamlom (2012). Irrelevant alterations in porosity degree are also observable in the AAM formulations. In this case, however, an opposite trend can be identified compared to OPC-based mixes. The effective compatibilization between rubber and geopolymer paste considerably reduced the impact of the interfacial voids on the global porosity of the material. Moreover, with the same sand-GTR and RP-RG ratios, the AAM-based samples showed φ-values lower than the Portland counterpart (except in the case of RP100 formulation where, in accordance with the standard deviations, comparable values are noted). Compared to the mix designs of OPC-based samples, the synthesis of geopolymer mortars involved a very small amount of water in the mixture, leading to lower capillary porosity [80]. Another possible reason for this difference is attributable to the self-compacting characteristics of the AAM mix designs, which would significantly enhance the densification of the materials (see the density comparison in Figure 11), also justifying the irrelevant impact of the GTR addition on φ and WA. The self-compaction behaviour of utilised AAM was verified throughout the author's previous researches (Chougan et al., 2020; Albar et al., 2020; Chougan et al., 2021). It was examined using comprehensive fresh property tests, including flow table, mini-slump, and rheology. The microstructural improvement related to the use of self-compacting binders was previously demonstrated by Bignozzi and Sandrolini (2006), who also verified the poor influence of rubber aggregates addition on porosity and water permeability.

WA results (Figure 12b) followed trends consistent with φ-values recorded in OPC and AAM mixes under investigation. WA values ranged between 9.31% to 13.32% in Portland-based formulations and between 8.3%

and 13.62% in AAM-based formulations. Although in accordance with BS 1881 (2015) technical standards these values appear higher than ordinary concrete (WA in the range 3% to 5%), numerous non-structural applications in the civil and building sectors can be satisfied, such as draining paving block for road surfaces or parking areas (Li et al., 2019b) and lightweight acoustic barriers (Arenas et al., 2017). Compared to the Portland formulations, the geopolymer ones overall exhibited a lower absorbent behavior attributable to the influence of GTR on the pore structure of the material.

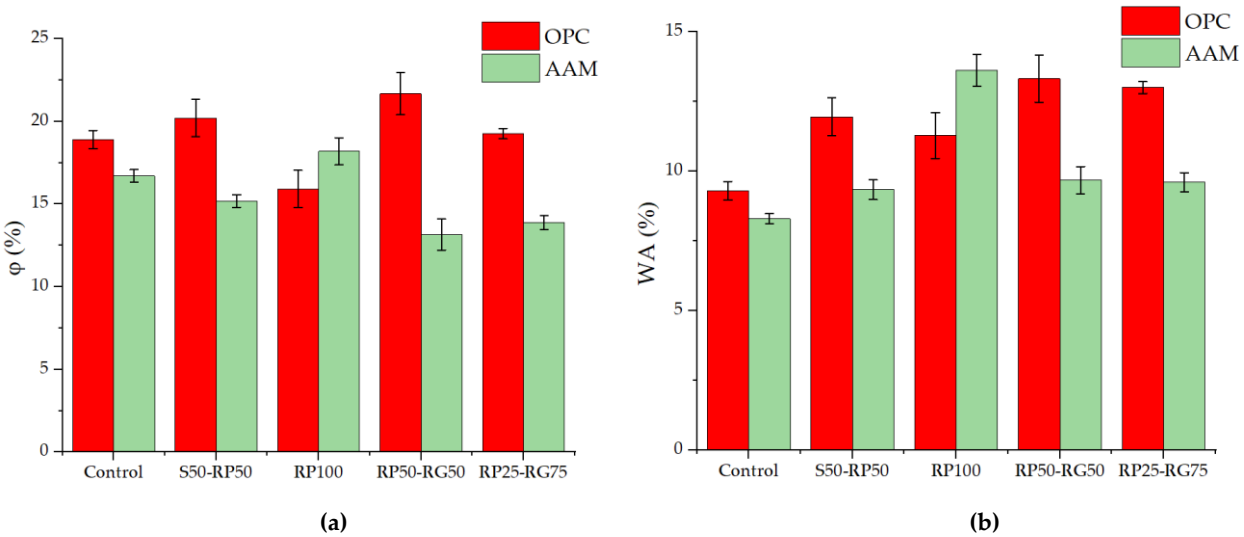


**Figure 12.** φ (a) and WA (b) test results of OPC and geopolymer mixes

### *3.5. Mechanical testing results*

#### *3.5.1. Compressive test*

Decay in mechanical strength induced by the addition of GTR in place of the mineral aggregates is common evidence deduced from research on rubber-concrete technology, both in the case of Portland (Roychand et al, 2020; Thomas and Gupta, 2016; Li et al., 2019c) and geopolymer matrices (Wongsa et al., 2018; Dong et al., 2021). From the cited works, strong consensus is demonstrable regarding the causes that lead to this mechanical loss: a) mismatching in deformability properties between concrete aggregates and rubber particles, resulting in high stress concentrations into the matrix ("air void-like" behaviour of rubber aggregates); b) weak rubber-matrix interfacial cohesion related to the morphology and chemical composition of GTR; c) lower strength properties of polymer aggregates than sand, resulting in an overall weakening of the cementitious composite; d) tendency of GTR aggregates to incorporate air bubbles during the fresh material mixing, implying an increasing in porosity. As illustrated in Figure 13, a gradual loss in compressive strength ($\sigma_c$) was noted as the volumetric level of GTR increases. The changes in $\sigma_c$-value followed the same trend in both the OPC and AAM binders. According to the density results described above, the highest reduction rate was found in the RP100 mix, while slight strength recovery was achieved by employing RG in the aggregate blend. The coarse polymer fraction would seem functional in terms of strength properties if equally balanced with RP (i.e., in RP50-RG50 mix) where, compared to the RP100 samples, increments in $\sigma_c$-value by 36.8% and 35% for OPC and AAM matrices were observed, respectively. In a previous study (Sambucci and Valente, 2021), the authors recognized the efficient influence of coarse rubber aggregate on the toughness and crack resistance performance. However, exceeding the RG content (RP25-RG75 mix), $\sigma_c$-value tended to decrease probably due to strong impact of the poor adhesion with the matrix.

To investigate the effect of GTR addition on the mechanical performance of the two matrices, the strength reduction rates for each formulation are reported. Starting from the plain samples with comparable strengths (53.75 MPa for Control-OPC and 49.10 MPa for Control-AAM), the following $\sigma_c$ -decreases were found: -56.7% in S50-RP50-OPC, -75.7% in RP100-OPC, -66.8% in RP50-RG50-OPC, -75.1% in RP25-RG75-OPC and -66.5% in

S50-RP50-AAM, -91.6% in RP100-AAM, -88.7% in RP50-RG50-AAM, -92% in RP25-RG75-AAM. From the mechanical analysis, it is evident that the Portland-based formulations perform better under compression than those AAM which are affected by stronger strength losses following the incorporation of GTR aggregates.

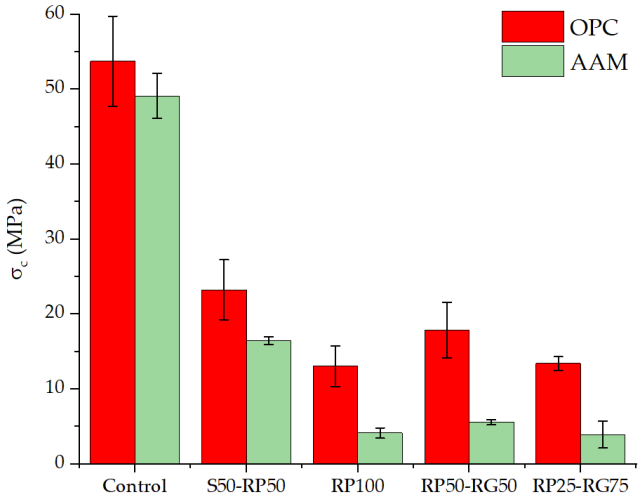


**Figure 13.** $\sigma_c$ results from compressive test

Two possible hypotheses can be provided to clarify the different impact of rubber modification on the mechanical performance of OPC and AAM mixes.

1) As anticipated in Section 3.3, the mineral aggregates (sand) make a significant influence on the mechanical and microstructural characteristics of the geopolymer, providing a supply of silica for the development of the aluminosilicate network. In this context, Si/Al ratio can be considered an indicator to evaluate the quality of the AAM-based concrete. Yusuf et al. (2014) reviewed a range of Si/Al ratio between 3.0 and 3.8 to obtain highest strength properties. Lower molar ratios tend to favor a brittle and highly crystalline microstructure consisting of a Si-O-Al network with low strength (Sambucci et al., 2021; Lahoti et al., 2017). An increase in Si/Al ratio results in a progressive growth in Si-O-Si bonds which are stronger than Si-O-Al bonds. This assists more amorphous and denser geopolymer microstructure (poly-sialate-siloxo network) with higher mechanical strength, also due to the promoted formation of silica particles that act as reinforcements (Sambucci et al., 2021; He et al., 2016). However, excessive Si/Al ratios promote the formation of the aluminosilicate gel in very early reaction times, hindering the proper microstructural development of the geopolymer matrix with consequent weakening of its mechanical performance (Criado et al., 2007). EDX investigation allowed a preliminary comparative analysis in terms of Si/Al ratio between plain and rubberized samples to evaluate alterations in chemical proportions resulting from the integration of the polymer aggregates. Specifically, Figure 14 relates $\sigma_c$ and Si/Al ratio in Control-AAM, S50-RP50-AAM, and RP100-AAM. The elemental ratio values are an average of four EDX scans performed on the geopolymer matrix under examination.

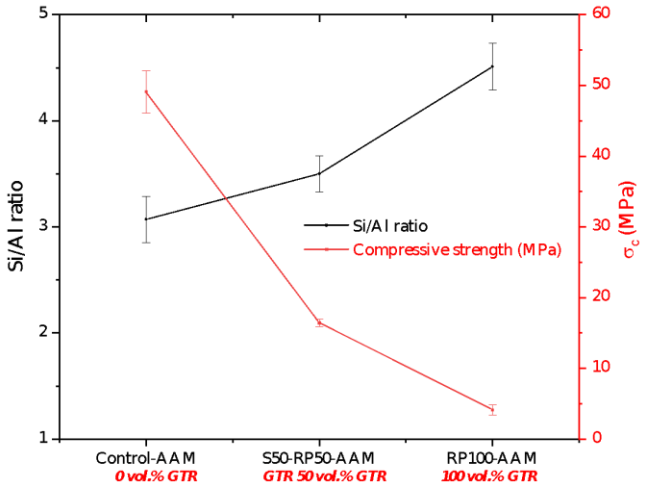


**Figure 14.** Relationship between $\sigma_c$ and Si/Al ratio in Control-AAM, S50-RP50-AAM, and RP100-AAM mixes

The strength reduction from Control-AAM to RP100-AAM is accompanied by a progressive increase in the Si/Al ratio. The gradual replacement of the mineral aggregates with GTR reduces the presence of active sites for activation by the alkaline solution. Therefore, the increase in Si/Al ratio is potentially attributable to an excess of silicate, deriving from the activator, inoperative on the proper development of aluminosilicate network. This effect does not lead to the onset of porosity in the matrix (as can also be observed from the trend in Figure 10a) but in a hindered strength gain by the material resulting from the reduced dissolution rate of the aluminate species, generally provided by the stone-based aggregates, and the silicate (Asif et al., 2015). Indeed, it is noted that the absence of sand in RP100-AAM mix shifts the elemental ratio outside the optimal range, confirming the influence of the sand on the mechanical and microstructural quality of the geopolymer samples.

2) Another argument for comparing OPC and AAM formulations could be that the OPC mix design is similar to a high-strength cement compounds, involving many chemical additives that can play a big role in maintaining optimal rheology properties, such as reduced water/cement ratios, and increasing the strength of the hardened materials.

*3.5.2. Three-point flexural test*

Flexural test results are reported in terms of flexural strength ($\sigma_f$), elastic modulus ($E_f$), and comparison of load-strain curves between OPC and AAM mixes.

According to Figure 15a, the strength reduction for $\sigma_f$ is in trend with that of $\sigma_c$, attributing the mechanical losses to the same reasons previously stated for the compressive behavior. However, the comparison between OPC and AAM samples highlights an opposite trend with respect to the compressive testing results. All geopolymer-based formulations appeared to be superior in terms of strength under flexural load. A possible argument for such experimental evidence is the following: the better interfacial properties found in AAM-based mixes ensure the effective load transfer from the matrix to the polymer filler and delay the pull-out of the GTR aggregate, significantly enhancing the toughness, anti-cracking ability, and flexural strength of the material. This deduction agrees with the rubber compatibilization investigations aimed at improving the mechanical performance of the rubberized concrete (Xie et al., 2019; Rivas-Vázquez et al., 2015). Therefore, it is possible to define two different mechanisms that affect the mechanical properties of rubberized AAM-based mixes: the compressive strength is mainly governed by the quality of the geopolymer matrix, while the flexural properties are optimized by the interfacial GTR-matrix cohesion.

As observed in Figure 15b, the reduction in $E_f$ was primarily due to the lower modulus of elasticity of GTR than sand. For both binders, $E_f$ was reduced with increased rubber amount (Atahan and Yücel, 2012; Turatsinze and Garros, 2008). In relation to the respective Control samples, having stiffness modulus of 5.56 GPa in OPC mix and 4.09 GPa in AAM mix, the partial sand-rubber volumetric replacement (S50-RP50 mix) resulted in reduction rates of 9.7% and 43.8% in OPC and AAM mixes, respectively. The complete sand-GTR replacement involved further fall in $E_f$ without significant alterations of the elasticity properties with the size gradation of the polymer aggregates. Totally rubberized OPC and AAM formulation had $E_f$ values in the range 1.82-1.94 GPa (maximum $E_f$ reduction of 67.3% in RP25-RG75-OPC) and 0.73-0.91 GPa (maximum $E_f$ reduction of 82.2% in RP100-AAM), respectively.

By comparing the $E_f$ reduction rates found in OPC and AAM samples, more marked percentage losses were noted in geopolymer-based mixes. This observation suggests that the flexible nature of rubber has greater control over the material's deformability than the stiff characteristic of the matrix, resulting from the better compatibility with the geopolymer paste and the consequent lower influence of the microstructural bond defects at the rubber-binder interface.

The lower $E_f$ of GTR-containing mortars confer greater deflection properties to the mortars. From the load-strain curves of OPC-based samples and AAM-based (Fig.15c) samples (Fig.15d), it was observed how the addition of polymer aggregates promotes the transition from a purely brittle features, typical in ceramic-cementitious materials, to a more ductile behavior that gradually enhances with the increase in the GTR volumetric level. The influence of RG was evident on the deformability properties. The highest performance in terms of elongation-at-break was found in RP25-RG75 mixes, confirming the functionality of coarser polymer particles on the material's toughness discussed in Section 3.1.2. Even in this case, the incorporation of rubber gave a specific mechanical response depending on the type of matrix, because of the different GTR-OPC and GTR-AAM interface adhesion properties. OPC-based rubberized mixes revealed elongation-at-break between 0.05% (S50-RP50-OPC sample) and less than 0.8% (RP25-RG75 sample). In AAM-based blends, the elastomeric functions of GTR aggregates appear strongly maximized, resulting in maximum fracturing strain about an order of magnitude higher than the Portland mixes. The improved deformability properties can be considered highly attractive in numerous non-structural precast products where the energy absorption, damping of vibro-acoustic stresses, and mechanical flexibility are primary requirements, such as paving block for sport facilities, flexible road pavement for non-traffic areas, and partition wall bricks with insulating properties.

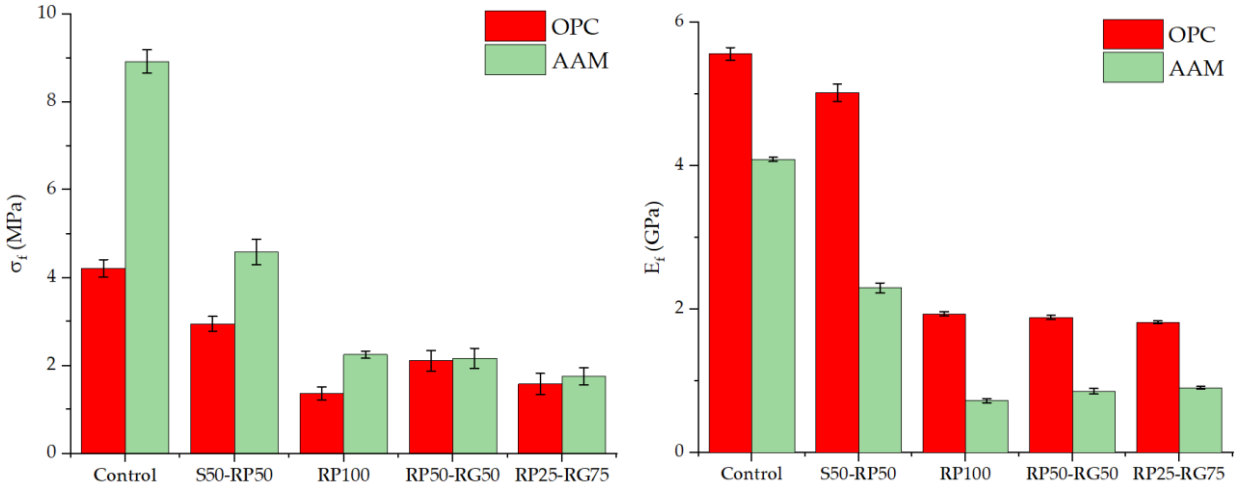


**(a)** **(b)**

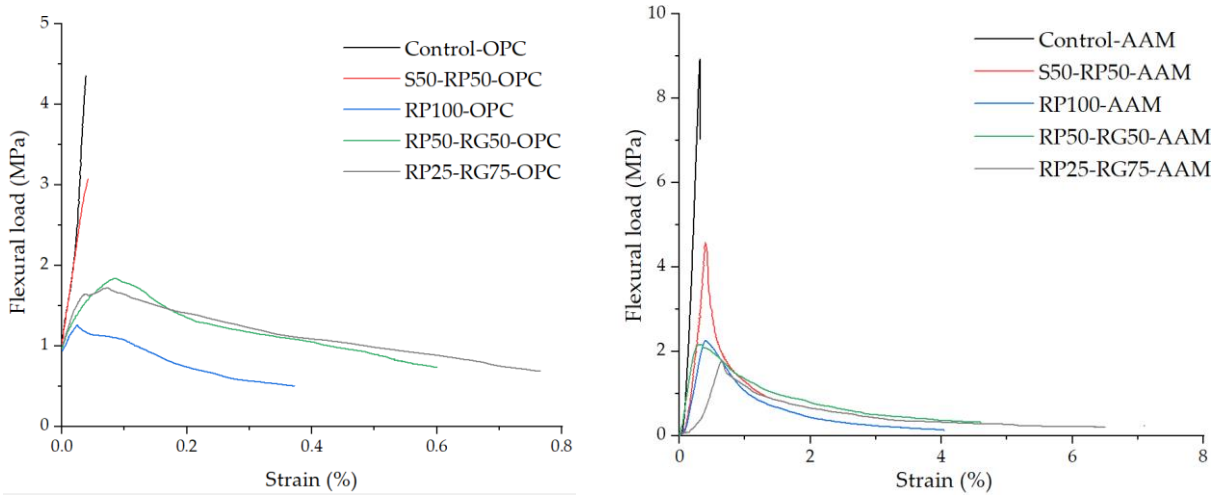


(c) (d)

**Figure 15.** Three-point flexural test results: $\sigma_f$ (a), $E_f$ (b), and load-displacement curves for OPC (c) and AAM (d) samples.

Figure 16 shows two micrographs acquired by optical microscopy, reporting the post-failure surfaces of RP25-RG75-OPC (Fig.16a) and RP25-RG75-AAM (Fig.16b) samples. The comparison was reported as additional evidence to verify different interfacial cohesion between rubber aggregates and the binders. When the rubber-cement bond is weak, the pull-out of the polymeric aggregate from the matrix (Fig.16a) strongly limits the material's deformability and the maximum strength is reached at lower deformation levels. Conversely, the good adhesion with the geopolymer matrix enables the full elastic functionality of GTR aggregates. In Figure 16b, the polymer aggregate maintains a proper adherence with both parts of the broken specimen, elongating according to the bending deformation to which the material was subjected. This demonstrates the correlation between matrix-polymer interface properties and higher toughness of AAM-based mixes than OPC ones.

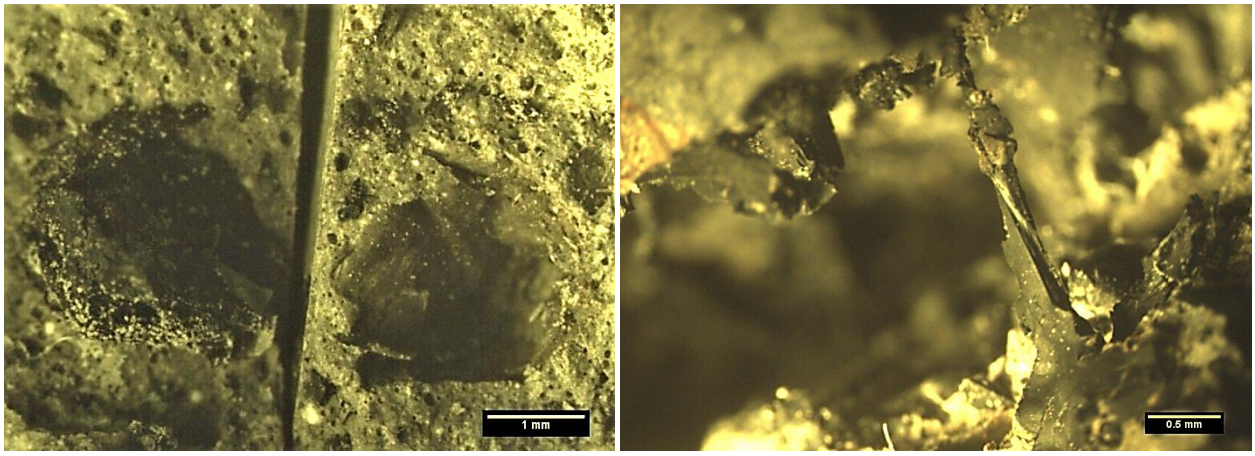


**(a)** **(b)**

**Figure 16.** Optical microscopy analysis of fracture surfaces after flexural test: RP25-RG75-OPC sample (a) and RP25-RG75-AAM (b)

### *3.6 $ECO_2$ emissions and cost analysis*

$ECO_2$ results are presented in Fig.17a. Regardless of the type of mix design, AAM binder developed in this study provided lower carbon emission levels than its Portland counterpart. Taking the results of the OPC mixtures as reference values, it is possible to note $ECO_2$ reduction rates close to 30% and 40% for Control-AAM and RP100-AAM mixes, respectively. This finding aligns well with the results reported in a previous review

754 work conducted by the authors (Valente et al., 2021), in which it was found that the AAM technology
755 represents a valid eco-sustainable solution to ordinary cement mixes, bringing on carbon emissions reduction
756 rates up to 80%. For both matrices, an increase in the carbon footprint was estimated by replacing the mineral
757 fraction with the tire rubber aggregate. In relation to Control formulations, the modified mix designs show an
758 increase in the $ECO_2$ index of approximately 52% (RP100-OPC) and 28% (RP100-AAM). However, this trend
759 is not directly attributed to the environmental impact induced by the processing GTR, which results more eco-
760 effective than the use of mineral aggregates, but to the higher content of raw materials (Portland cement and
761 aluminosilicate binders/alkali activator) required. The results fit with a previous LCA study conducted by
762 Maxineasa et al. (2017), which verified an approximately 5% increase in $CO_2$ emissions by producing concrete
763 mixes containing recycled rubber particles as partial aggregate replacement (40 vol.%). Opposite findings were
764 proved by Medine et al. (2020) research, where low substitution rates of mineral aggregates with rubber ones
765 (up to 10 w/w%) induced slight reductions in $CO_2$ emissions (0.24-0.48%) compared to an ordinary concrete
766 mix. Accordingly, by considering low content of GTR would be inefficient both in terms of technological
767 properties and environmental impact and it would therefore be worth emphasizing the research on making
768 the matrices more sustainable to incorporate high volume of recycled rubber. In agreement with the $ECO_2$
769 results obtained, GTR would seem to perform better in AAM matrices, whose eco-impact is mainly related to
770 the production of the alkaline activator (about 90% of the overall emission contribution). In this regard, by
771 working on a "cleaner" AAM mix design, for example through the implementation of "one-part geopolymer
772 technology" (Ouellet-Plamondon and Habert, 2015), more favourable levels of eco-sustainability could be
773 achieved.

774 The basic ingredients used to design the present AAM formulation raised the production cost of the final
775 material (Fig.17b), confirming literature finding on cost analysis comparison between geopolymeric and
776 Portland concrete materials (McLellan et al., 2011; Shang et al., 2018). The role of GTR on the cost computation
777 is strictly dependent on the sand market rates. With the available data, two different trends can be defined:
778 for the RP100-OPC mix production, rubber addition reduces the costs deriving from the aggregate fraction by
779 approximately 28%, while for RP100-AAM mix the GTR aggregate involves a price 2.5 times higher than the
780 mineral one. However, caution is recommended when generalising the results since the study is referred to
781 two different contexts, i.e. Italian and British, and the price of the aggregates could be subjected to relevant
782 variations. Based on the experimental results previously presented, rubberized AAM mixes demonstrated
783 some competitive/better performance compared with OPC-based cementitious composites, thus requiring less
784 material to obtain equal structural stability. Geopolymers are also subjected to a lower carbon emission
785 taxation regime as a potential means of supporting low-carbon solutions. Furthermore, in accordance with
786 current national and international eco-sustainable policy aimed at preserving the natural resources, the cost
787 of traditional aggregates is likely to increase in future. Therefore, the use of recycled rubber materials for
788 targeted civil-architectural applications where their functionality can be strongly enhanced (lightweight
789 precast elements, pavement units with improved ductility, thermal-noise blocking blocks in building) (Medina
790 et al., 2018), may be a more cost-effective option in the near future. All of these can help to level the cost gap
791 between OPC and geopolymer cementitious composites.

792

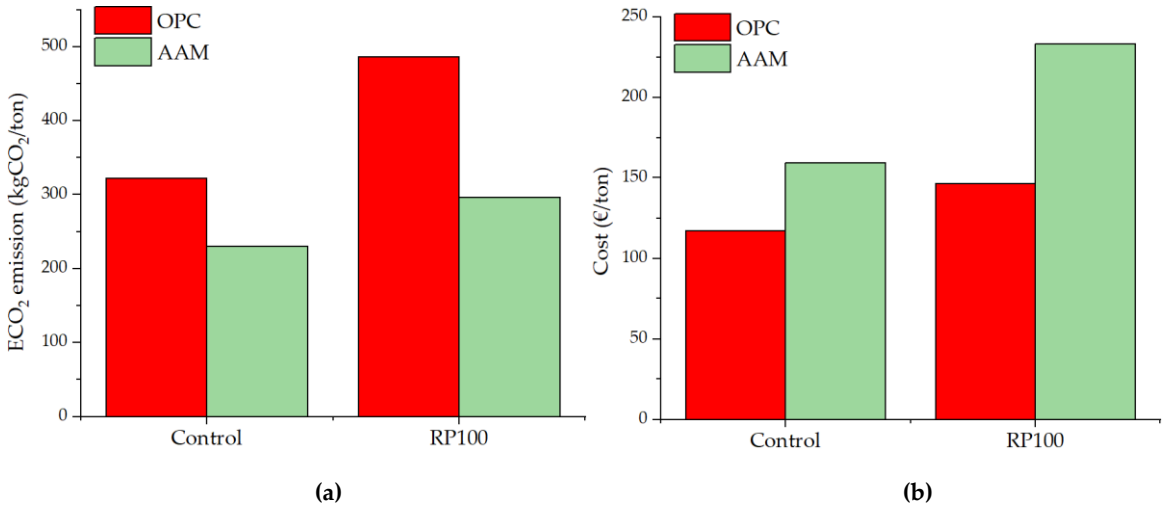


**Figure 17.** $ECO_2$ emission (a) and cost analysis (b): Comparison between plain and rubberized concrete considering OPC and AAM matrices.

## 4. Conclusions and future directions

The use of recycled rubber, deriving from end-of-life tires, as an aggregate in AAM mixes is a novel approach that goes well with the current eco-sustainable proposals of the cement and concrete industry. This work reported a comparative analysis between OPC and FA-GGBS-SF geopolymer mortars functionalized with GTR, investigating different sand-rubber replacement levels, and evaluating the influence of two size gradation of polymer aggregates (0-1 mm RP and 1-3 mm RG). According to the experimental results, the following conclusions could be drawn.

1. Microstructural analysis shows a marked difference in interfacial adhesion of GTR aggregates with the two binder systems. An improved GTR-matrix compatibility was observed in the geopolymer mixes due to the synergistic effect of NaOH and SF on the instinct chemical-physical functionalization of rubber, inducing a superior ductile behavior under bending.

2. The porosity rate and permeability of the mixes were affected by varied microstructural characteristics in terms of rubber-matrix interfacial adhesion. Although the incorporation of GTR led to a slight increase in the φ and WA in both matrices, the geopolymer formulations showed lower values than the OPC counterparts. As a further hypothesis, the reduced water content used in the mix design of the AAM formulations, and their self-compacting behaviour could minimize the effect of permeable porosity in the hardened samples

3. The addition of GTR involves a predictable decrease in unit weight and mechanical strength with the increasing the sand-rubber replacement level. However, the geopolymer formulations show stronger drops than the OPC ones, in terms of density and compressive strength. As confirmed by EDX analysis, the reason must be associated with the crucial role of mineral aggregates like Si-source in the structural quality of the geopolymer matrix.

4. The addition of the coarse fraction (RG) allows to recover the strength properties of the samples and effectively acts on the crack-delaying behavior and deformability properties. However, its content should be balanced to avoid the significant impact of interface defects on porosity and loss of mechanical strength.

5. From the available P and EC data, it has been estimated that the AAM matrices are more environmental-effective but slightly expensive than the OPC. By totally replacing the sand with the rubber aggregates, increases are identified both in terms of carbon emissions and of overall cost, mainly associated with the higher quantity of binder required to produce the rubberized mixes.

Considering the promising characteristics of the developed AAM-GTR mixes, based on this preliminary investigation, future research works will be aimed at optimization studies of the geopolymer mix design, working on the synthesis variables that significantly affect the microstructural and mechanical quality of the material (Si/Al ratio and therefore, activator molarity, and use of Si-rich precursors). Moreover, further characterization of the rubberized geopolymer formulations will be performed to explore the technological performances, such as dynamic mechanical properties, thermo-acoustic insulation, and durability, where the functionality of tire rubber aggregates is strongly valued. Addressing the next studies on the design of cleaner matrices and promoting the use of recycled rubber materials in concrete applications could lead to a cost-emission gap levelling between Portland and geopolymer rubber-based composites

## CRediT authorship contribution statement

**Marco Valente:** Conceptualization, Supervision, Visualization, Writing – Review & Editing, Project administration. **Matteo Sambucci:** Conceptualization, Methodology, Validation, Investigation, Formal analysis, Writing - Original draft**. Mehdi Chougan**: Conceptualization, Investigation, Validation, Formal analysis, Writing – Review & Editing. **Seyed Hamidreza Ghaffar:** Conceptualization**,** Supervision, Visualization, Writing – Review & Editing, Project administration.

## Declaration of competing interest

The authors declare that they have no known competing financial interests or personal relationships that could have appeared to influence the work reported in this paper.

## Acknowledgements

The authors would like to express their sincere gratitude to Eng. Ettore Musacchi (ETRA) for the supply of the ground tire rubber used in the research activity and Prof. Paola Russo and Dr. Sofia Ubaldi (Department of Chemical Engineering, Materials, Environment, Sapienza University of Rome) for the technical assistance in the ATR-FTIR chemical analysis.

## References

[1] Damineli, B. L., Kemeid, F. M., Aguiar, P. S., & John, V. M. (2010). Measuring the eco-efficiency of cement use. *Cement and Concrete Composites*, *32*(8), 555-562. https://doi.org/10.1016/j.cemconcomp.2010.07.009

[2] Ali, M. B., Saidur, R., & Hossain, M. S. (2011). A review on emission analysis in cement industries. *Renewable and Sustainable Energy Reviews*, *15*(5), 2252-2261. https://doi.org/10.1016/j.rser.2011.02.014

[3] Naik, T. R. (2005). Sustainability of the cement and concrete industries. *Sustainable construction materials and technologies*, 19-25. https://doi.org/10.1680/asic.34044.0017

[4] Sheheryar, M., Rehan, R., & Nehdi, M. L. (2021). Estimating CO2 Emission Savings from Ultrahigh Performance Concrete: A System Dynamics Approach. *Materials*, *14*(4), 995. https://doi.org/10.3390/ma14040995

[5] Xi, F., Davis, S. J., Ciais, P., Crawford-Brown, D., Guan, D., Pade, C., ... & Liu, Z. (2016). Substantial global carbon uptake by cement carbonation. *Nature Geoscience*, *9*(12), 880-883. https://doi.org/10.1038/ngeo2840

[6] Golewski, G. L. (2020). Energy savings associated with the use of fly ash and nanoadditives in the cement composition. *Energies*, *13*(9), 2184. https://doi.org/10.3390/en13092184

[7] Dhondy, T., Remennikov, A., & Shiekh, M. N. (2019). Benefits of using sea sand and seawater in concrete: a comprehensive review. *Australian Journal of Structural Engineering*, *20*(4), 280-289. https://doi.org/10.1080/13287982.2019.1659213

[8] EEA. European Environmental Agency. Available online: https://www.eea.europa.eu/publications/cutting-greenhouse-gas-emissions-through

[9] J. Davidovits. The need to create a new technical language for the transfer of basic scientific information. Transfer and Exploitation of Scientific and Technical Information Luxembourg. Commission of the European Communities (1982), p. 7716.

[10] Sambucci, M., Sibai, A., & Valente, M. (2021). Recent Advances in Geopolymer Technology. A Potential Eco-Friendly Solution in the Construction Materials Industry: A Review. *Journal of Composites Science*, *5*(4), 109. https://doi.org/10.3390/jcs5040109

[11] Duxson, P., Fernández-Jiménez, A., Provis, J. L., Lukey, G. C., Palomo, A., & van Deventer, J. S. (2007). Geopolymer technology: the current state of the art. *Journal of materials science*, *42*(9), 2917-2933. https://doi.org/10.1007/s10853-006-0637-z

[12] Provis, J. L., & Van Deventer, J. S. J. (Eds.). (2009). *Geopolymers: structures, processing, properties and industrial applications*. Elsevier.

[13] Marvila, M. T., Azevedo, A. R. G. D., & Vieira, C. M. F. (2021). Reaction mechanisms of alkali-activated materials. *Revista IBRACON de Estruturas e Materiais*, *14*. https://doi.org/10.1590/S1983-41952021000300009

[14] Wastiels, J., Wu, X., Faignet, S., Patfoort, G., & Zandi, I. (1994). Mineral polymer based on fly ash. *Journal of Resource Management and Technology*, *22*, 135-141.

[15] Zhang, P., Gao, Z., Wang, J., Guo, J., Hu, S., & Ling, Y. (2020). Properties of fresh and hardened fly ash/slag based geopolymer concrete: A review. *Journal of Cleaner Production*, 122389. https://doi.org/10.1016/j.jclepro.2020.122389

[16] Amran, M., Debbarma, S., & Ozbakkaloglu, T. (2021). Fly ash-based eco-friendly geopolymer concrete: A critical review of the long-term durability properties. *Construction and Building Materials*, *270*, 121857. https://doi.org/10.1016/j.conbuildmat.2020.121857

[17] McLellan, B. C., Williams, R. P., Lay, J., Van Riessen, A., & Corder, G. D. (2011). Costs and carbon emissions for geopolymer pastes in comparison to ordinary portland cement. *Journal of cleaner production*, *19*(9-10), 1080-1090. https://doi.org/10.1016/j.jclepro.2011.02.010

[18] Ouellet-Plamondon, C., & Habert, G. (2015). Life cycle assessment (LCA) of alkali-activated cements and concretes. In *Handbook of alkali-activated cements, mortars and concretes* (pp. 663-686). Woodhead Publishing. https://doi.org/10.1533/9781782422884.5.663

[19] Meshram, R. B., & Kumar, S. (2021). Comparative life cycle assessment (LCA) of geopolymer cement manufacturing with Portland cement in Indian context. *International Journal of Environmental Science and Technology*, 1-12. https://doi.org/10.1007/s13762-021-03336-9

[20] Nath, S. K., & Kumar, S. (2020). Role of particle fineness on engineering properties and microstructure of fly ash derived geopolymer. *Construction and Building Materials*, 233, 117294. https://doi.org/10.1016/j.conbuildmat.2019.117294

[21] Kumar, S., & Kumar, R. (2014). Geopolymer: cement for low carbon economy. *Indian Concr J*, 88, 29-37. http://www.icjonline.com/icj_z_Home_techPapers_vie.

[22] Nuruddin, M. F., Malkawi, A. B., Fauzi, A., Mohammed, B. S., & Almattarneh, H. M. (2016, June). Geopolymer concrete for structural use: Recent findings and limitations. In *IOP Conference Series: Materials Science and Engineering* (Vol. 133, No. 1, p. 012021). IOP Publishing. https://doi.org/10.1088/1757-899X/133/1/012021

[23] Part, W. K., Ramli, M., & Cheah, C. B. (2015). An overview on the influence of various factors on the properties of geopolymer concrete derived from industrial by-products. *Construction and Building Materials*, *77*, 370-395. https://doi.org/10.1016/j.conbuildmat.2014.12.065

[24] Wang, Y. S., Alrefaei, Y., & Dai, J. G. (2019). Silico-aluminophosphate and alkali-aluminosilicate geopolymers: A comparative review. *Frontiers in Materials*, *6*, 106. https://doi.org/10.3389/fmats.2019.00106

[25] Van Deventer, J. S., Provis, J. L., & Duxson, P. (2012). Technical and commercial progress in the adoption of geopolymer cement. *Minerals Engineering*, *29*, 89-104. https://doi.org/10.1016/j.mineng.2011.09.009

[26] Fernandez-Jimenez, A., & Palomo, A. (2009). Chemical durability of geopolymers. In *Geopolymers* (pp. 167-193). Woodhead Publishing.

[27] Pacheco-Torgal, F., Abdollahnejad, Z., Miraldo, S., & Kheradmand, M. (2017). Alkali-activated cement-based binders (AACB) as durable and cost-competitive low-CO 2 binder materials: some shortcomings that need to be addressed. *Handbook of low carbon concrete*, 195-216. http://dx.doi.org/10.1016/B978-0-12-804524-4.00009-9

[28] Xiao, R., Jiang, X., Zhang, M., Polaczyk, P., & Huang, B. (2020a). Analytical investigation of phase assemblages of alkali-activated materials in CaO-SiO2-Al2O3 systems: The management of reaction products and designing of precursors. *Materials & Design*, *194*, 108975. https://doi.org/10.1016/j.matdes.2020.108975

[29] Xiao, R., Zhang, Y., Jiang, X., Polaczyk, P., Ma, Y., & Huang, B. (2021). Alkali-activated slag supplemented with waste glass powder: Laboratory characterization, thermodynamic modelling and sustainability analysis. *Journal of Cleaner Production*, *286*, 125554. https://doi.org/10.1016/j.jclepro.2020.125554

[30] Mohajerani, A., Suter, D., Jeffrey-Bailey, T., Song, T., Arulrajah, A., Horpibulsuk, S., & Law, D. (2019). Recycling waste materials in geopolymer concrete. *Clean Technologies and Environmental Policy*, 21(3), 493-515. https://doi.org/10.1007/s10098-018-01660-2

[31] Lim, Y. Y., Pham, T. M., & Kumar, J. (2021). Sustainable alkali activated concrete with fly ash and waste marble aggregates: Strength and Durability studies. *Construction and Building Materials,* 283, 122795. https://doi.org/10.1016/j.conbuildmat.2021.122795

[32] Dave, S., Bhogayata, A., & Arora, D. N. (2017). Impact resistance of geopolymer concrete containing recycled plastic aggregates. *EasyChair*, 1, 137-143. https://doi.org/10.29007/nwsh

[33] De Rossi, A., Ribeiro, M. J., Labrincha, J. A., Novais, R. M., Hotza, D., & Moreira, R. F. P. M. (2019). Effect of the particle size range of construction and demolition waste on the fresh and hardened-state properties of

947 fly ash-based geopolymer mortars with total replacement of sand. *Process Safety and Environmental*
948 *Protection*, *129*, 130-137. https://doi.org/10.1016/j.psep.2019.06.026

949 [34] Hajimohammadi, A., Ngo, T., & Kashani, A. (2018). Glass waste versus sand as aggregates: The
950 characteristics of the evolving geopolymer binders. *Journal of Cleaner Production*, *193*, 593-603.
951 https://doi.org/10.1016/j.jclepro.2018.05.086

952 [35] Xiao, R., Polaczyk, P., Zhang, M., Jiang, X., Zhang, Y., Huang, B., & Hu, W. (2020b). Evaluation of glass
953 powder-based geopolymer stabilized road bases containing recycled waste glass aggregate. *Transportation*
954 *Research Record*, *2674*(1), 22-32. https://doi.org/10.1177/0361198119898695

955 [36] Roychand, R., Gravina, R. J., Zhuge, Y., Ma, X., Youssf, O., & Mills, J. E. (2020). A comprehensive review
956 on the mechanical properties of waste tire rubber concrete. *Construction and Building Materials*, 237, 117651.
957 https://doi.org/10.1016/j.conbuildmat.2019.117651

958 [37] Thomas, B. S., & Gupta, R. C. (2016). A comprehensive review on the applications of waste tire rubber in
959 cement concrete. *Renewable and Sustainable Energy Reviews*, 54, 1323-1333.
960 https://doi.org/10.1016/j.rser.2015.10.092

961 [38] Huang, B., Li, G., Pang, S. S., & Eggers, J. (2004). Investigation into waste tire rubber-filled concrete.
962 *Journal of Materials in Civil Engineering*, 16(3), 187-194. https://doi.org/10.1061/(ASCE)0899-1561(2004)16:3(187)

963 [39] Anwar Khitab, S. A., Arif, I., Awan, F. A., Anwar, A., Mughal, A., & Awan, H. A. (2017). Evaluation of
964 concrete with partial replacement of coarse aggregates by waste rubber. *International journal for innovative*
965 *research in multidisciplinary field*, *3*, 12.

966 [40] Aly, A. M., El-Feky, M. S., Kohail, M., & Nasr, E. S. A. (2019). Performance of geopolymer concrete
967 containing recycled rubber. *Construction and Building Materials*, 207, 136-144.
968 https://doi.org/10.1016/j.conbuildmat.2019.02.121

969 [41] Wongsa, A., Sata, V., Nematollahi, B., Sanjayan, J., & Chindaprasirt, P. (2018). Mechanical and thermal
970 properties of lightweight geopolymer mortar incorporating crumb rubber. *Journal of Cleaner Production*, 195,
971 1069-1080. https://doi.org/10.1016/j.jclepro.2018.06.003

972 [42] Dong, M., Elchalakani, M., Karrech, A., & Yang, B. (2021). Strength and durability of geopolymer
973 concrete with high volume rubber replacement. *Construction and Building Materials*, *274*, 121783.
974 https://doi.org/10.1016/j.conbuildmat.2020.121783

975 [43] Lazorenko, G., Kasprzhitskii, A., & Mischinenko, V. (2021). Rubberized geopolymer composites: Effect
976 of filler surface treatment. *Journal of Environmental Chemical Engineering*, *9*(4), 105601.
977 https://doi.org/10.1016/j.jece.2021.105601

978 [44] ADOT. Available online: https://apps.azdot.gov/files/materials-manuals/materials-testing/ariz-714c.pdf.

979 [45] Valente, M., Sambucci, M., Sibai, A., & Musacchi, E. (2020). Multi-physics analysis for rubber-cement
980 applications in building and architectural fields: A preliminary analysis. *Sustainability*, *12*(15), 5993.
981 https://doi.org/10.3390/su12155993

982 [46] Wik, A., & Dave, G. (2009). Occurrence and effects of tire wear particles in the environment–A critical
983 review and an initial risk assessment. *Environmental pollution*, *157*(1), 1-11.
984 https://doi.org/10.1016/j.envpol.2008.09.028

985 [47] Youssf, O., Mills, J. E., & Hassanli, R. (2016). Assessment of the mechanical performance of crumb
986 rubber concrete. *Construction and Building Materials*, *125*, 175-183.
987 https://doi.org/10.1016/j.conbuildmat.2016.08.040

[48] Sambucci, M., Marini, D., Sibai, A., & Valente, M. (2020). Preliminary Mechanical Analysis of Rubber-Cement Composites Suitable for Additive Process Construction. *Journal of Composites Science*, *4*(3), 120. https://doi.org/10.3390/jcs4030120

[49] BS EN 450-1:2012. Fly ash for concrete. Definition, specifications, and conformity criteria. London, UK: British Standards Institution

[50] Chougan, M., Ghaffar, S. H., Jahanzat, M., Albar, A., Mujaddedi, N., & Swash, R. (2020). The influence of nano-additives in strengthening mechanical performance of 3D printed multi-binder geopolymer composites. *Construction and Building Materials*, *250*, 118928. https://doi.org/10.1016/j.conbuildmat.2020.118928

[51] Albar, A., Chougan, M., Al-Kheetan, M. J., Swash, M. R., & Ghaffar, S. H. (2020). Effective extrusion-based 3D printing system design for cementitious-based materials. *Results in Engineering*, *6*, 100135. https://doi.org/10.1016/j.rineng.2020.100135

[52] Chougan, M., Ghaffar, S. H., Sikora, P., Chung, S. Y., Rucinska, T., Stephan, D., ... & Swash, M. R. (2021). Investigation of additive incorporation on rheological, microstructural and mechanical properties of 3D printable alkali-activated materials. *Materials & Design*, *202*, 109574. https://doi.org/10.1016/j.matdes.2021.109574

[53] BS 410-1 (2000). Test sieves: Technical requirements and testing – Part 1: Test sieves of metal wire cloth. London, UK: British Standards Institution

[54] ASTM C 1202. Standard test method for electrical indication of concrete's ability to resist chloride ion penetration. Annual Book of ASTM Standards, vol. 04.02, American Society of Testing and Materials, Philadelphia (2002)

[55] ASTM International. Standard Test Method for Compressive Strength of Hydraulic Cement Mortars (Using 2-in. or [50-mm] Cube Specimens); ASTM C109/C109M-20a; ASTM International: West Conshohocken, PA, USA, 2020

[56] ASTM International. Standard Test Method for Flexural Strength of Hydraulic-Cement Mortars; ASTM C348-20; ASTM International: West Conshohocken, PA, USA, 2020.

[57] Bostanci, S. C., Limbachiya, M., & Kew, H. (2018). Use of recycled aggregates for low carbon and cost effective concrete construction. *Journal of Cleaner Production*, *189*, 176-196. https://doi.org/10.1016/j.jclepro.2018.04.090

[58] EPDItaly. Available online: https://www.epditaly.it/

[59] EFCA. Available online: https://swe.sika.com/dms/getdocument.get/60b7f6a6-92fc-36b7-ae01-45e0c48e395d/SuperplasticizerED.pdf

[60] Botto, S. (2009). Tap water vs. bottled water in a footprint integrated approach. *Nature precedings*, 1-1. https://doi.org/10.1038/npre.2009.3407.1

[61] Dal Pozzo, A., Carabba, L., Bignozzi, M. C., & Tugnoli, A. (2019). Life cycle assessment of a geopolymer mixture for fireproofing applications. *The International Journal of Life cycle Assessment*, *24*(10), 1743-1757. https://doi.org/10.1007/s11367-019-01603-z

[62] Petrillo, A., Cioffi, R., Ferone, C., Colangelo, F., & Borrelli, C. (2016). Eco-sustainable geopolymer concrete blocks production process. *Agriculture and agricultural science procedia*, *8*, 408-418. https://doi.org/10.1016/j.aaspro.2016.02.037

[63] Rashid, K., Yazdanbakhsh, A., & Rehman, M. U. (2019). Sustainable selection of the concrete incorporating recycled tire aggregate to be used as medium to low strength material. *Journal of Cleaner Production*, *224*, 396-410. https://doi.org/10.1016/j.jclepro.2019.03.197

[64] Kong, D. L., Sanjayan, J. G., & Sagoe-Crentsil, K. (2007). Comparative performance of geopolymers made with metakaolin and fly ash after exposure to elevated temperatures. *Cement and concrete research*, *37*(12), 1583-1589. https://doi.org/10.1016/j.cemconres.2007.08.021

[65] Kramar, S., & Ducman, V. (2015). Mechanical and microstructural characterization of geopolymer synthesized from low calcium fly ash. *Chemical Industry and Chemical Engineering Quarterly*, *21*(1-1), 13-22. https://doi.org/10.2298/CICEQ130725042K

[66] Li, Y., Zhang, X., Wang, R., & Lei, Y. (2019a). Performance enhancement of rubberised concrete via surface modification of rubber: A review. *Construction and Building Materials*, *227*, 116691. https://doi.org/10.1016/j.conbuildmat.2019.116691

[67] Xie, J., Li, J., Lu, Z., Li, Z., Fang, C., Huang, L., & Li, L. (2019). Combination effects of rubber and silica fume on the fracture behaviour of steel-fibre recycled aggregate concrete. *Construction and Building Materials*, *203*, 164-173. https://doi.org/10.1016/j.conbuildmat.2019.01.094

[68] Langan, B. W., Weng, K., & Ward, M. A. (2002). Effect of silica fume and fly ash on heat of hydration of Portland cement. *Cement and Concrete research*, *32*(7), 1045-1051. https://doi.org/10.1016/S0008-8846(02)00742-1

[69] Guo, Q., Zhang, R., Luo, Q., Wu, H., Sun, H., & Ye, Y. (2019). Prediction on damage evolution of recycled crumb rubber concrete using quantitative cloud imagine correlation. *Construction and Building Materials*, *209*, 340-353. https://doi.org/10.1016/j.conbuildmat.2019.03.115

[70] Lanzón, M., Cnudde, V., De Kock, T., & Dewanckele, J. (2015). Microstructural examination and potential application of rendering mortars made of tire rubber and expanded polystyrene wastes. *Construction and building materials*, *94*, 817-825. https://doi.org/10.1016/j.conbuildmat.2015.07.086

[71] Parande, A. K., Babu, B. R., Pandi, K., Karthikeyan, M. S., & Palaniswamy, N. (2011). Environmental effects on concrete using Ordinary and Pozzolana Portland cement. *Construction and Building Materials*, *25*(1), 288-297. https://doi.org/10.1016/j.conbuildmat.2010.06.027

[72] Rees, C. A., Provis, J. L., Lukey, G. C., & Van Deventer, J. S. (2007). In situ ATR-FTIR study of the early stages of fly ash geopolymer gel formation. *Langmuir*, *23*(17), 9076-9082. https://doi.org/10.1021/la701185g

[73] Parsaie, A., Tamsilian, Y., Pordanjani, M. R., Abadshapoori, A. K., & McKay, G. (2021). Novel approach for rapid oil/water separation through superhydrophobic/superoleophilic zinc stearate coated polyurethane sponges. *Colloids and Surfaces A: Physicochemical and Engineering Aspects*, *618*, 126395. https://doi.org/10.1016/j.colsurfa.2021.126395

[74] Mermerdaş, K., Manguri, S., Nassani, D. E., & Oleiwi, S. M. (2017). Effect of aggregate properties on the mechanical and absorption characteristics of geopolymer mortar. *Engineering science and Technology, an international Journal*, *20*(6), 1642-1652. https://doi.org/10.1016/j.jestch.2017.11.009

[75] Arellano-Aguilar, R., Burciaga-Díaz, O., Gorokhovsky, A., & Escalante-García, J. I. (2014). Geopolymer mortars based on a low grade metakaolin: Effects of the chemical composition, temperature and aggregate: binder ratio. *Construction and Building Materials*, *50*, 642-648. https://doi.org/10.1016/j.conbuildmat.2013.10.023

[76] Angelin, A. F., Lintz, R. C. C., Gachet-Barbosa, L. A., & Osorio, W. R. (2017). The effects of porosity on mechanical behavior and water absorption of an environmentally friendly cement mortar with recycled rubber. *Construction and Building Materials*, *151*, 534-545. https://doi.org/10.1016/j.conbuildmat.2017.06.061

[77] Girskas, G., & Nagrockienė, D. (2017). Crushed rubber waste impact of concrete basic properties. *Construction and Building Materials*, *140*, 36-42. https://doi.org/10.1016/j.conbuildmat.2017.02.107

[78] Di Mundo, R., Dilonardo, E., Nacucchi, M., Carbone, G., & Notarnicola, M. (2019). Water absorption in rubber-cement composites: 3D structure investigation by X-ray computed-tomography. *Construction and Building Materials*, *228*, 116602. https://doi.org/10.1016/j.conbuildmat.2019.07.328

[79] Sukontasukkul, P., & Tiamlom, K. (2012). Expansion under water and drying shrinkage of rubberized concrete mixed with crumb rubber with different size. *Construction and Building Materials*, *29*, 520-526. https://doi.org/10.1016/j.conbuildmat.2011.07.032

[80] M. Olivia, P. Sarker, H. Nikraz. (2008, June). Water Penetrability of low calcium fly ash geopolymer concrete. In *Proceedings of the International Conference on Construction and Building Technology* (pp. 517-530). http://repository.unri.ac.id:80/handle/123456789/3577

[81] Bignozzi, M. C., & Sandrolini, F. (2006). Tyre rubber waste recycling in self-compacting concrete. *Cement and concrete research*, *36*(4), 735-739. https://doi.org/10.1016/j.cemconres.2005.12.011

[82] BS 1881 (2015). Testing Concrete. Methods for analysis of hardened concrete. London, UK: British Standards Institution

[83] Li, D., Toghroli, A., Shariati, M., Sajedi, F., Bui, D. T., Kianmehr, P., ... & Khorami, M. (2019b). Application of polymer, silica-fume and crushed rubber in the production of Pervious concrete. *Smart Struct. Syst*, *23*(2), 207-214. https://doi.org/10.12989/sss.2019.23.2.207

[84] Arenas, C., Luna-Galiano, Y., Leiva, C., Vilches, L. F., Arroyo, F., Villegas, R., & Fernández-Pereira, C. (2017). Development of a fly ash-based geopolymeric concrete with construction and demolition wastes as aggregates in acoustic barriers. *Construction and Building Materials*, *134*, 433-442. https://doi.org/10.1016/j.conbuildmat.2016.12.119

[85] Li, Y., Zhang, S., Wang, R., & Dang, F. (2019c). Potential use of waste tire rubber as aggregate in cement concrete–A comprehensive review. *Construction and Building Materials*, *225*, 1183-1201. https://doi.org/10.1016/j.conbuildmat.2019.07.198

[86] Sambucci, M., & Valente, M. (2021). Influence of Waste Tire Rubber Particles Size on the Microstructural, Mechanical, and Acoustic Insulation Properties of 3D-Printable Cement Mortars. *Civil Engineering Journal*, *7*(6), 937-952. 10.28991/cej-2021-03091701

[87] Yusuf, M. O., Johari, M. A. M., Ahmad, Z. A., & Maslehuddin, M. (2014). Effects of addition of Al (OH) 3 on the strength of alkaline activated ground blast furnace slag-ultrafine palm oil fuel ash (AAGU) based binder. *Construction and Building Materials*, *50*, 361-367. https://doi.org/10.1016/j.conbuildmat.2013.09.054

[88] Lahoti, M., Narang, P., Tan, K. H., & Yang, E. H. (2017). Mix design factors and strength prediction of metakaolin-based geopolymer. *Ceramics International*, *43*(14), 11433-11441. https://doi.org/10.1016/j.ceramint.2017.06.006

[89] He, P., Wang, M., Fu, S., Jia, D., Yan, S., Yuan, J., ... & Zhou, Y. (2016). Effects of Si/Al ratio on the structure and properties of metakaolin based geopolymer. *Ceramics international*, *42*(13), 14416-14422. https://doi.org/10.1016/j.ceramint.2016.06.033

[90] Criado, M., Fernández-Jiménez, A., & Palomo, A. (2007). Alkali activation of fly ash: Effect of the SiO2/Na2O ratio: Part I: FTIR study. *Microporous and mesoporous materials*, *106*(1-3), 180-191. https://doi.org/10.1016/j.micromeso.2007.02.055

[91] A. Asif, M. Zakaria, K.A.M. Azizli, M.F. Nuruddin, L. Ismail. The effect of Si/Al ratio and sodium silicate on the mechanical properties of fly ash based geopolymer for coating. Mater. Sci. Forum, 803 (2015), pp. 355-361. https://doi.org/10.4028/www.scientific.net/MSF.803.355

[92] Rivas-Vázquez, L. P., Suárez-Orduña, R., Hernández-Torres, J., & Aquino-Bolaños, E. (2015). Effect of the surface treatment of recycled rubber on the mechanical strength of composite concrete/rubber. *Materials and Structures*, *48*(9), 2809-2814. https://doi.org/10.1617/s11527-014-0355-y

[93] Atahan, A. O., & Yücel, A. Ö. (2012). Crumb rubber in concrete: static and dynamic evaluation. *Construction and Building Materials*, *36*, 617-622. https://doi.org/10.1016/j.conbuildmat.2012.04.068

[94] Turatsinze, A., & Garros, M. (2008). On the modulus of elasticity and strain capacity of self-compacting concrete incorporating rubber aggregates. *Resources, conservation and recycling*, *52*(10), 1209-1215. https://doi.org/10.1016/j.resconrec.2008.06.012

[95] Valente, M., Sambucci, M., & Sibai, A. (2021). Geopolymers vs. Cement Matrix Materials: How Nanofiller Can Help a Sustainability Approach for Smart Construction Applications—A Review. *Nanomaterials*, *11*(8), 2007. https://doi.org/10.3390/nano11082007

[96] Maxineasa, S. G., Neocleous, K., Dumitrescu, L., Themistocleous, K., Taranu, N., & Hadjimitsis, D. G. (2017). Environmental LCA of innovative reuse of all End-of-life tyre components in concrete. Proceedings of the *1st International Conference on Construction Materials for Sustainable Future*, Zadar, Croatia, 19 - 21 April 2017, ISBN: 978-953-8168-04-8, pp 941-947. https://ktisis.cut.ac.cy/handle/10488/13404

[97] Medine, M., Trouzine, H., de Aguiar, J. B., & Djadouni, H. (2020). Life cycle assessment of concrete incorporating scrap tire rubber: comparative study. *Nature & Technology*, (23), 1-11. https://www.asjp.cerist.dz/en/Articles/47

[98] Shang, J., Dai, J. G., Zhao, T. J., Guo, S. Y., Zhang, P., & Mu, B. (2018). Alternation of traditional cement mortars using fly ash-based geopolymer mortars modified by slag. *Journal of cleaner production*, *203*, 746-756. https://doi.org/10.1016/j.jclepro.2018.08.255

[99] Medina, N. F., Garcia, R., Hajirasouliha, I., Pilakoutas, K., Guadagnini, M., & Raffoul, S. (2018). Composites with recycled rubber aggregates: Properties and opportunities in construction. *Construction and Building Materials*, *188*, 884-897. https://doi.org/10.1016/j.conbuildmat.2018.08.069